POLITECNICO DI TORINO
Repository ISTITUZIONALE

Survey and Sequence Strategies for Full3D Electrical Resistivity Tomography in Archaeological Sites: A Case Study on a

Original
Survey and Sequence Strategies for Full3D Electrical Resistivity Tomography in Archaeological Sites: A Case Study on a
Domus
of the Roman Town of Augusta Bagiennorum (NW Italy) / Vergnano, A., Franco, D., Merico, A., Pace, F., Uggè, S., Comina, C.. - In: ARCHAELOGICAL PROSPECTION. - ISSN 1075-2196. - 33:1(2026), pp. 87-107. [10.1002/arp.70013]
Availability:
This version is available at: 11583/3010856 since: 2026-05-15T12:11:55Z

Publisher:
Wiley

Published
DOI:10.1002/arp.70013

Terms of use:

This article is made available under terms and conditions as specified in the corresponding bibliographic description in the repository

Publisher copyright

(Article begins on next page)

28 November 2026

Check for updates

Archaeological Prospection

WILEY

RESEARCH ARTICLE OPEN ACCESS

Survey and Sequence Strategies for Full-3D Electrical Resistivity Tomography in Archaeological Sites: A Case Study on a *Domus* of the Roman Town of Augusta Bagiennorum (NW Italy)

Andrea Vergnano[1] | Diego Franco[2] | Antonio Merico[1] | Francesca Pace[2] | Sofia Uggè[3] | Cesare Comina[1]

[1]Department of Earth Sciences, University of Turin, Turin, Italy | [2]Department of Environment, Land and Infrastructure Engineering, Polytechnic of Turin, Turin, Italy | [3]Residenze Reali Sabaude—Direzione Regionale Musei Nazionali del Piemonte, Turin, Italy

Correspondence: Andrea Vergnano (andrea.vergnano@unito.it)

Received: 24 April 2025 | **Revised:** 5 September 2025 | **Accepted:** 8 September 2025

Funding: The authors received no specific funding for this work.

Keywords: 3D ERT | archaeogeophysics | GPR

ABSTRACT

Preliminary geophysical investigations are a cost-effective and efficient way to screen archaeological sites and locate buried structures. Ground-penetrating radar (GPR) is one of the most widely used methods for archaeological prospection, but in some sites, it cannot be employed effectively due to the presence of clay or other electrically conductive materials, which strongly attenuate the electromagnetic signal, or due to bumped terrain, which demands rigorous signal analysis. Alternatively, electrical resistivity tomography (ERT) can be adopted in these situations. However, ERT is not as frequently adopted as GPR for archaeological purposes because it is more time and cost consuming and, generally, has worse resolution. In this study, we aim to test a full-3D ERT approach to improve the imaging quality of ERT surveys for archaeological prospections. We develop specific survey strategies, including a custom open-source quadrupole sequence generator, studied for achieving high sensitivity to archaeological remains within the first metres of subsoil. We performed a test survey on a well-known archaeological site (the Roman town of Augusta Bagiennorum, NW Italy) and compared the results with a state-of-the-art multichannel GPR acquisition. The results showed that both GPR and ERT equally located the outer and inner walls of a complex Roman residential building. Moreover, the ERT could locate two targets, barely visible in the GPR survey, with the antenna used. We also compared the results of our full-3D ERT approach to a more common quasi-3D approach. We found that the full-3D approach overcomes the directional bias found in our quasi-3D acquisitions and provides a more accurate subsurface resistivity model. This methodology is ready to be employed in other archaeological sites and, differently from GPR, can easily operate on bumped terrain, in the presence of clay, and potentially reach greater investigation depths.

1 | Introduction

Preliminary geophysical investigations are usually employed to rapidly locate buried structures with a lower economic and logistical effort than direct digging (Witten 2017). These investigations are particularly beneficial when there is the need to avoid disturbing archaeological evidence that might affect the timeline and cost of construction for infrastructure or buildings. In state-owned archaeological areas, like the one in this case study, preliminary geophysical surveys also play a crucial role in accurately estimating excavation costs and determining the extent of excavation work needed for archaeological

This is an open access article under the terms of the Creative Commons Attribution License, which permits use, distribution and reproduction in any medium, provided the original work is properly cited.

© 2025 The Author(s). *Archaeological Prospection* published by John Wiley & Sons Ltd.

research projects. Among the different techniques, geomagnetometry and ground-penetrating radar (GPR) are the most employed (Linford 2006). Geomagnetometry has been used for a long time for the detection and mapping of buried remains at large archaeological sites (Clark 1996; David et al. 2008). GPR has been increasingly appreciated, especially in the last decade, due to the introduction of multichannel systems that, thanks to a full 3D reconstruction of the investigated sites, allow for locating buried structures up to 1–2 m of depth with a very high resolution (Trinks et al. 2018). However, GPR is not suitable for all environments. Its accuracy and investigation depth decrease if the subsurface is rich in clay, due to its peculiar electrical properties that significantly attenuate the electromagnetic waves (De Domenico et al. 2006; Wunderlich and Rabbel 2013). Similarly, the signal is attenuated also if subsoil has high water content (e.g., Conyers 2018).

Instead, electrical resistivity tomography (ERT) does not face similar issues in clayish soils, where it can easily distinguish the shallow resistive anomalies (e.g., buried walls) in a conductive background. Also, ERT measurements can potentially reach greater investigation depths than GPR in similar environments, depending on the adopted antenna frequencies, and be used more easily on slopes or bumped terrain. However, ERT generally has a worse resolution than GPR, requires increased acquisition costs and times, and it is difficult to find an ERT survey report in which buried structures are depicted as clearly as in GPR surveys.

Traditionally, ERT surveys have been conducted along straight lines and interpreted as sections or profiles in 2D. However, the 2D interpretation of buried structures, which often have complex 3D geometries, can lead to misleading results, and many efforts have been undertaken to recognize and quantify this bias (Loke 2004; Berge and Drahor 2011a; Arosio et al. 2018; Bièvre et al. 2018; Boyd et al. 2019; Hojat et al. 2020; Hojat 2024; Hung et al. 2019). Therefore, to identify the shape of archaeological remains, there is a need to increase the ERT data density to obtain 3D data volumes, which can be cut into depth slices, similarly to GPR. In the last decades, archaeological research has often carried out 3D ERT interpretation adopting mainly three different strategies:

1. acquiring single 2D longitudinal or transverse lines and invert them in 3D, what we call 'quasi 3D'as in Negri et al. 2008; Leucci and Greco 2012; D. L. Argote-Espino et al. 2016; Fernández-Álvarez et al. 2017; Al-Saadi et al. 2018; Loke, Papadopoulos, et al. 2020; Gaber et al. 2021; N. Papadopoulos et al. 2021; Lu et al. 2023;
2. acquiring combined 2D longitudinal and transverse lines and invert them in 3D, what we call 'conventional 3D', following the strategy suggested by the guidelines of Loke 2004, but seldom employed due to the increased acquisition times, as in N. G. Papadopoulos et al. 2007;
3. acquiring different electrode combinations over a 3D grid comprising in-line and off-line electrodes and invert all the data in 3D, what we call 'full 3D' as in Louvaris et al. 2025.

However, full-3D ERT surveys for archaeological purposes are still rare: an example using 48 electrodes in a 6 × 8 m grid inside a cave to investigate prehistoric remains is reported by Torrese et al. (2022); another example in a crypt is reported by Vásconez-Maza et al. (2020). A notable full-3D approach, the 'Maximum Yield Grid' (MYG), involved using two separate instruments to control the current and potential dipoles arranged in a grid. This approach is based on a number of potential electrodes that is about 15 times greater than the number of current electrodes to minimize the acquisition time and enhance the logistics while maintaining a good resolution (Capizzi et al. 2012; Casas et al. 2018; Fiandaca et al. 2010).

Other works dealt with unusual 3D geometries, for example, investigating the subsurface below a large building by placing the electrodes around the structure, or employing the so-called 'perimeter arrays' quadrupole sequences (D. Argote-Espino et al. 2013; Chávez et al. 2018; Abdullah et al. 2019; García-Nieto et al. 2024). Also, a radial arrangement of electrodes to investigate archaeological *tumuli* has been adopted (N. G. Papadopoulos et al. 2010; Tsourlos et al. 2014; Karaoulis et al. 2025).

Research has also explored semi-automatic and automatic acquisition strategies to speed up the otherwise slow ERT surveys. N. G. Papadopoulos et al. 2006 presented an efficient survey setup to perform shallow-depth pole-pole ERTs. An automatic acquisition technique, automatic resistivity profiling (ARP), has also been developed to acquire ERT data from a vehicle along investigation lines (Dabas 2008). These approaches allow only shallow investigation depths but are generally sufficient for archaeological prospections (N. G. Papadopoulos et al. 2009).

The 3D ERT approaches reviewed above are many, because most ERT surveys have to find a compromise between limited time, complex logistics and results quality. The quasi-3D approach is simple, but may introduce directional biases that may hamper results quality. This is solved by employing the conventional-3D approach, at the cost of doubling the acquisition time. The acquisition times may be greatly reduced by automatic acquisition systems, but they only shine on flat large areas, whereas many archaeological sites have harsh terrain, bushes or other obstacles. Moreover, due to their fixed electrode geometry, they often offer limited investigation depth (which is, however, generally suitable for archaeological investigations). The full-3D approach offers the highest flexibility, resolution and investigation depth, but requires an instrument that handles around 100 or more electrodes to be effective, with acquisition times comparable to the quasi-3D approach.

Full-3D ERT acquisitions using several electrodes must develop suitable quadrupole sequences, because performing all the possible measurements would require too long acquisition time. Because the 3D ERT is a relatively new concept, there is still no standardized sequence such as the Wenner–Schlumberger or the dipole–dipole, which are very common in 2D surveys. A good 3D quadrupole sequence aims to find a compromise between a fast acquisition and an optimal spatial sensitivity, and this balance often depends on the survey goals and geometry (Stummer et al. 2004). Some optimization methods have been developed for this aim (Slob 2004; Wilkinson, Loke, et al. 2012; Loke, Wilkinson, et al. 2014; Simyrdanis et al. 2021; Qiang et al. 2022). The quadrupole sequence has been optimized for time-lapse analyses at the

10990763, 0, Downloaded from https://onlinelibrary.wiley.com/doi/10.1002/arp.70013 by Politecnico Di Torino Sist. Bibl Del Polit Di Torino, Wiley Online Library on [09/10/2025]. See the Terms and Conditions (https://onlinelibrary.wiley.com/terms-and-conditions) on Wiley Online Library for rules of use; OA articles are governed by the applicable Creative Commons License

lab scale (Sambuelli and Comina 2010) and at the field scale (Wilkinson, Uhlemann, et al. 2015), for borehole acquisitions (Al Hagrey 2012), for L-shaped, C-shaped or 'loop' electrode arrangements around buildings (Fischanger et al. 2007), for horizontally-layered subsoil with surface and borehole electrodes (Furman et al. 2007), for identifying the extension of the conductive leachate at the bottom of a landfill (Martorana et al. 2017) and for a 3D acquisition on an embankment slope (Uhlemann et al. 2018). To our knowledge, no sequence specifically developed for archaeological investigations is present in literature.

Moreover, rigorous sequence optimization strategies have the following shortcomings: (1) They are highly time consuming, particularly given the increase of available measuring electrodes in the modern ERT systems; as an example, the approach proposed by Loke, Wilkinson, et al. 2014 is recommended for less than 100 electrodes and generally the starting comprehensive dataset, necessary for the optimization, has a growth factor equal to the number of electrodes elevated to the power of four; (2) they are model dependent and should therefore be computed again for each new survey and each new subsoil condition; (3) they are often aimed at obtaining a uniform sensitivity to a significant depth, which may not always be the case in archaeology, where the investigation depths of interest are shallower (depending on the application); (4) with the increasing use of modern acquisition devices, which enable the simultaneous measurement of different potential dipoles given the same current dipole, removing some of the measurements through the optimization may not always lower the acquisition times.

In this context, this study aims to develop a full-3D ERT approach using a dense grid of current/potential electrodes, trying to decrease investigation times as much as possible, still retaining a good resolution. In the specific test site investigated in this study, we aimed to obtain the best possible resolution at shallow depths because the main archaeological remains are expected in the first two metres of subsoil. We focus on an efficient ERT survey setup and develop a fast quadrupole sequences generator that can be used for future archaeological prospections with similar grid geometries and in any test site. The quadrupole sequence was not 'optimized' in the sense described above, yet it comprehends every possible quadrupole that investigates the shallowest depths, retaining an acquisition time of less than 1 h. The ERT capability to locate the buried structures is tested and compared with the results from a multichannel GPR acquisition carried out over the same area. Comparison between ERT and GPR data has already been proposed in the literature (e.g., Lu et al. 2023). The difference between a full-3D and a quasi-3D approach is also evaluated and discussed.

We tested our survey approach on a 35 m × 15 m area in the archaeological park of Augusta Bagiennorum in the Piedmont region, NW Italy. This archaeological park is a well-known and important Roman site, extensively investigated since the end of the 19th century, both with detailed excavations and geophysical surveys (Assandria and Vacchetta 1925; Preacco 2014; Colombero et al. 2021; Vergnano et al. 2025). Its archaeological relevance is related to the absence of specific geomorphological constraints or pre-existing settlements that therefore enabled the application of a particularly rigorous urban planning scheme, exemplary compared with the canons developed in the Augustan Age (Preacco 2014). This planning scheme is also well preserved due to the absence of structures belonging to medieval or modern times, due to the abandonment of the urban centre in the early Middle Ages. This makes Augusta Bagiennorum an ideal site to increase the understanding of the urban topography of the minor centres of the Augustan Age and of their private and public areas. Previous surveys already evidenced several interesting structures, mainly pertaining to public areas and buildings (i.e., the *forum*, *capitolium* and *basilica*), and a clear link between vegetation cropmarks in satellite and aerial images and buried structures (Vergnano et al. 2025). The area specifically investigated in this study hosts a buried, well-preserved structure, possibly related to a complex Roman residential building.

2 | Methods

This section explains the proposed 3D ERT acquisition scheme, the survey setup, the sequence creation, and the preliminary tests performed before the field campaign. It also introduces the experimental approach to data inversion, the processing of complementary GPR data, acquired for comparison, and the comparison of the full-3D approach with a quasi-3D approach.

Given the extension of the investigated area and the available instrumentation, we opted to work with 144 steel electrodes in an 8 × 18 rectangular grid. The electrodes were spaced 2 m apart, covering an area of 14 m × 34 m, slightly less than the expected dimensions of the Roman residential building. The survey grid was then translated to a second acquisition over the same area to improve the resolution, as commented hereafter.

2.1 | Quadrupole Sequence

The quadrupole sequence for the ERT survey was designed to obtain a high information density near the surface. The buried structures are indeed expected to lie within the first two metres of subsoil, according to the previous GPR measurements at the same site (Vergnano et al. 2025). Therefore, we focused on quadrupoles with a short distance between the current and potential electrodes (less than 6 m), which generally correspond to shallower investigation depths.

Figure 1 shows a few graphical examples of current and potential electrodes used in the sequence. A script in R environment was written to create the desired sequence automatically, with the following strategy:

1. A series of current electrodes is defined, choosing all the possible current dipoles spaced 2 m, horizontally and vertically (e.g., yellow electrodes 143–144 in Figure 1). All the possible current dipoles spaced 6 m, horizontally and vertically, are also chosen (e.g., yellow electrodes 49–96 in Figure 1). The addition of other current dipoles was tested in forward simulations, with no particular improvements.

10990763, 0, Downloaded from https://onlinelibrary.wiley.com/doi/10.1002/arp.70013 by Politecnico Di Torino Sist. Bibl Del Polit Di Torino, Wiley Online Library on [09/10/2025]. See the Terms and Conditions (https://onlinelibrary.wiley.com/terms-and-conditions) on Wiley Online Library for rules of use; OA articles are governed by the applicable Creative Commons License

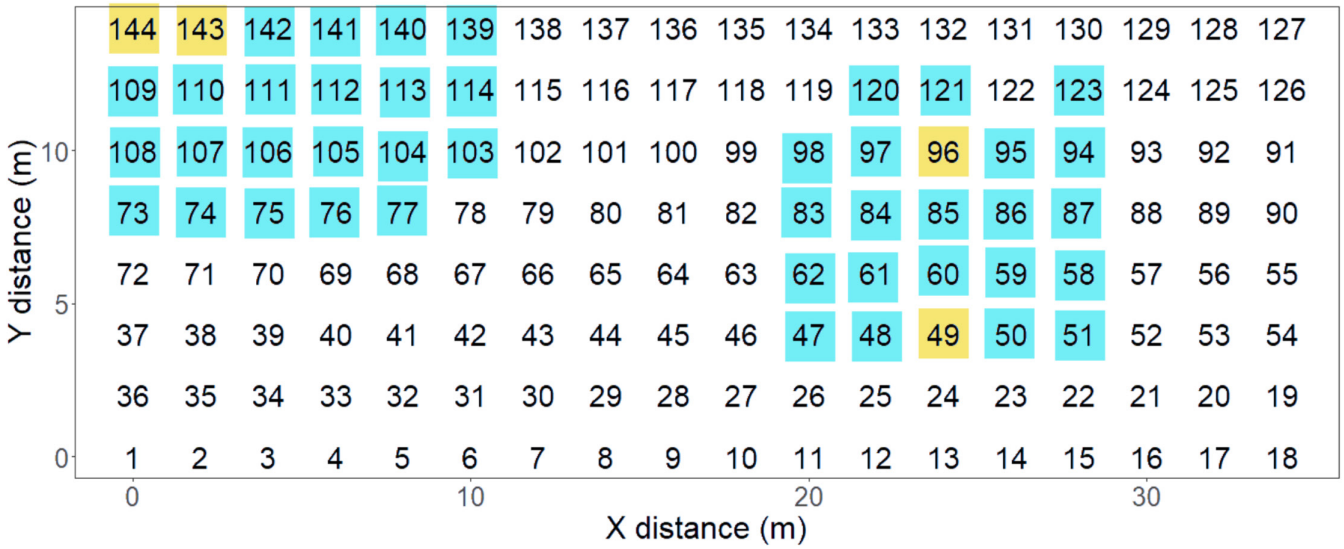


FIGURE 1 | 3D ERT acquisition scheme with the 144 numbered electrodes: example of two current dipoles (in yellow) and relative potential measurements (in light blue) over the planned survey grid.

2. For each current dipole, a series of 20 potential dipoles (light blue in Figure 1) is chosen among those around the current dipole, in a snake-like fashion. We do not employ known electrode arrays, such as equatorial dipole, because we are not interested in achieving an overall good resolution at all depths. Instead, with our custom sequence, we ensure maximum resolution for shallow depths, which are the main target for this (and similar) archaeological investigation. Because the adopted instrumentation can perform up to 10 measurements simultaneously, the 20 potential measurements are performed with just two current injections, provided that the potential dipoles are concatenated correctly.

For the example current dipoles in Figure 1, the light blue potential electrodes surrounding them give an indication of the maximum and minimum distance between the adopted electrodes, which is linked to the maximum investigation depth and the minimum and maximum resolution. The finally obtained sequence consisted of 9440 measurements. This acquisition approach ensured that many 'reverse' quadrupoles (i.e., with switched current and potential electrodes) existed in the sequence. These were later used in the inversion software to assess the measurement errors.

We then rearranged the sequence to make the current electrodes wait for a few measurements before being used as potential electrodes to minimize polarization effects that may introduce measurement errors (A. J. Wilkinson et al. 2006; Wilkinson, Loke, et al. 2012). This was performed automatically using an open-source script written in Fortran. All the scripts that create and optimize the sequence, commented in detail, are available open source in the Supporting Information (folder 'Main_sequence_scripts') of the paper and at https://github.com/Andrea-Vergnano/geophysics-utils, and can be reused for similar archaeological surveys focusing on shallow investigation depths, with any survey grid geometry and with reduced polarization errors in quadrupole sequences. The sequence itself is also available in the Supporting Information.

2.2 | Instruments and Survey Setup

We connected the electrodes to the georesistivimeter (72-channel Syscal Pro, manufactured by IRIS instruments) and two extensions (Switches, one with 48 channels and the other with 24 channels), thanks to six 24-channel cables, as illustrated in Figure 2. Electrodes from 1 to 72 were connected to the base Syscal Pro by means of three cables (yellow, green and blue lines in Figure 2). Electrodes from 73 to 120 were connected to the first Switch (orange and purple lines in Figure 2). Electrodes from 121 to 144 were connected to the second Switch (acid-green line in Figure 2).

The electrodes' positions were georeferenced thanks to a centimetre-accurate GNSS receiver with RTK corrections (Reach RS2+, manufactured by Emlid). After the first acquisition (see green circles in Figure 3), the grid was moved 1 m right and 1 m up (red circles in Figure 3), and the acquisition was repeated. This strategy was meant to increase the lateral (and not vertical) resolution quickly in a logistically convenient way, as verified in forward simulations (see Appendix A).

Six people took about 1 h to set up the acquisition layout (i.e., electrodes and cables), about half an hour to move the grid, and about 40 min to complete each acquisition of 9440 measurements. The instrument injected current for 250 ms by setting a potential difference of a maximum of 200 V between the current electrodes, then measured the potential difference between the potential electrodes. At least three measurements were performed and averaged for each quadrupole; if the standard deviation between them exceeded 2%, up to six measurements were performed.

We based the positioning of the grid according to the vegetation cropmarks seen from balloon and satellite images (see Figure 4a). However, we slightly mismatched the position of the grid so that the electrodes (yellow dots in Figure 4a) did not fully cover the bottom right exterior wall of the Roman residential building (bottom-right corner of the electrode distribution in

10990763, 0, Downloaded from https://onlinelibrary.wiley.com/doi/10.1002/arp.70013 by Politecnico Di Torino Sist. Bibl Del Polit Di Torino, Wiley Online Library on [09/10/2025]. See the Terms and Conditions (https://onlinelibrary.wiley.com/terms-and-conditions) on Wiley Online Library for rules of use; OA articles are governed by the applicable Creative Commons License

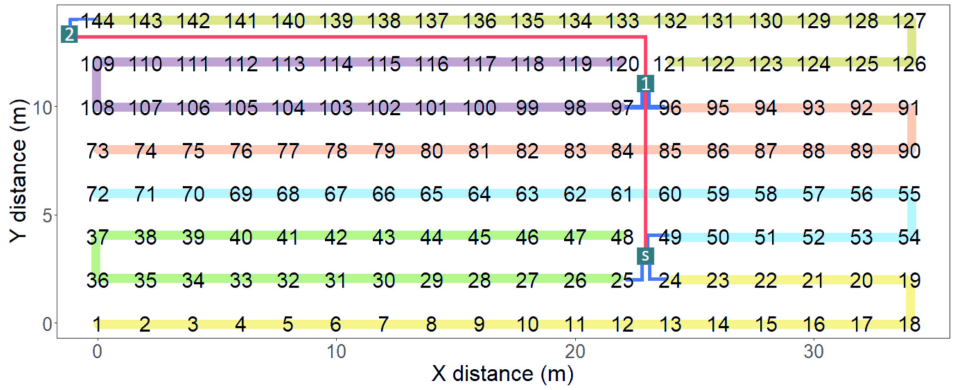


FIGURE 2 | 3D ERT acquisition scheme: The different cables are pictured in different colours. 'S', '1' and '2' blue squares are the Syscal georesistivimeter and its extensions, the Switch 1 and the Switch 2, respectively. The red lines represent the connections between the instruments (Syscal and Switches). The blue lines represent the connections between the instruments and the cables.

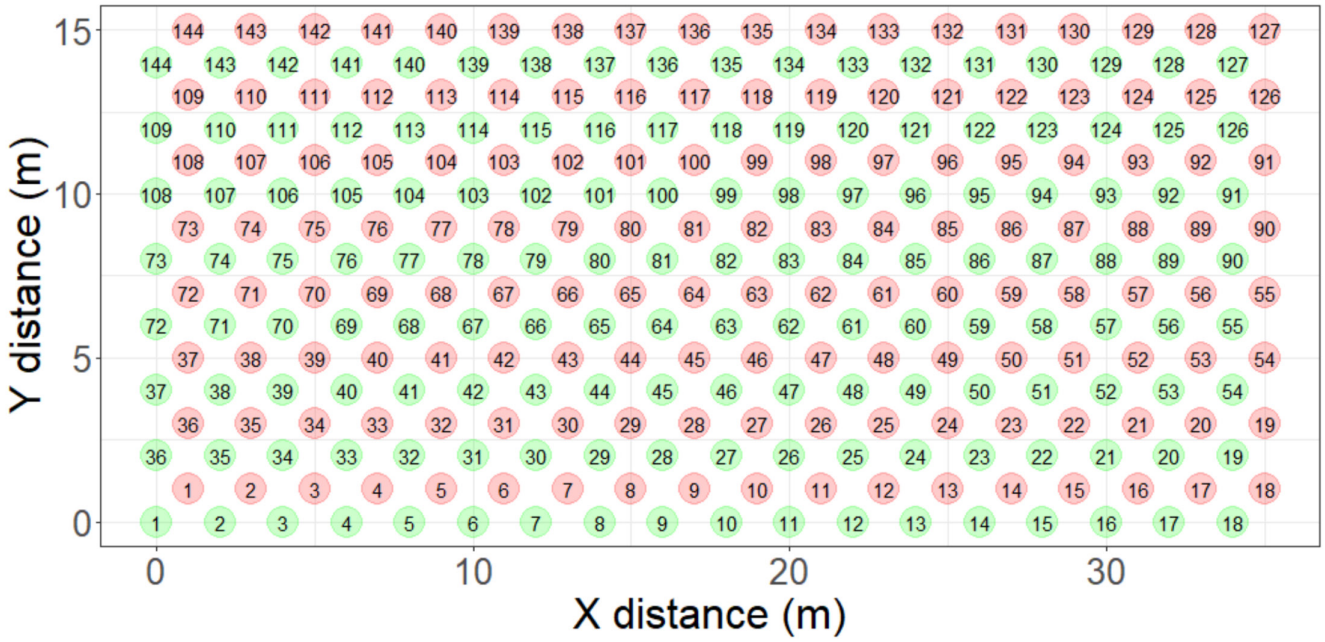


FIGURE 3 | 3D ERT acquisition scheme: electrode positions of the two overlapped surveys. The first acquisition is in green, the second acquisition in red.

Figure 4a). During the survey, the field was clear of vegetation, and the weather was sunny. However, the month before was very rainy, so the soil was still quite wet (Figure 4b).

2.3 | Data Processing and Inversion

The raw ERT data were filtered using Prosys III, a freeware proprietary program of the instrument manufacturer (Iris Instruments 2024). A few data points (only about 5%) were removed (due to, e.g., too high measured resistivity outliers, stacking error > 5%).

The inversions were carried out using ResIPy (Blanchy et al. 2020). The filtered data were imported, and the electrodes' positions were assigned to each electrode based on RTK GNSS georeferencing. The 'reverse' measurements were used to calculate a power-law error model that the inversion algorithm needs to know to evaluate the satisfactory mismatch between observed and calculated data.

The mesh used for inversion was automatically created with characteristic length of 0.2 m (about the expected thickness of the minor walls) and a growth factor of 5, setting the limit between fine and coarse mesh at 3 m depth. The tool used for mesh creation was GMSH (Geuzaine and Remacle 2009).

The 3D inversion was a regularized inversion with linear filtering and normal regularization. Further details on the parameters used for the inversion are available in the 'R3.in' text file or in the '.resipy' project, available in the Supporting Information ('inversions' folder). To assess the reliability of the final results, a sensitivity analysis was carried out (see Appendix A).

The results of the 3D ERT inversion were imported into Paraview 5.13.1 (Hansen and Johnson 2005) as a meshed

10990763, 0, Downloaded from https://onlinelibrary.wiley.com/doi/10.1002/arp.70013 by Politecnico Di Torino Sist. Bibl Del Polit Di Torino, Wiley Online Library on [09/10/2025]. See the Terms and Conditions (https://onlinelibrary.wiley.com/terms-and-conditions) on Wiley Online Library for rules of use; OA articles are governed by the applicable Creative Commons License

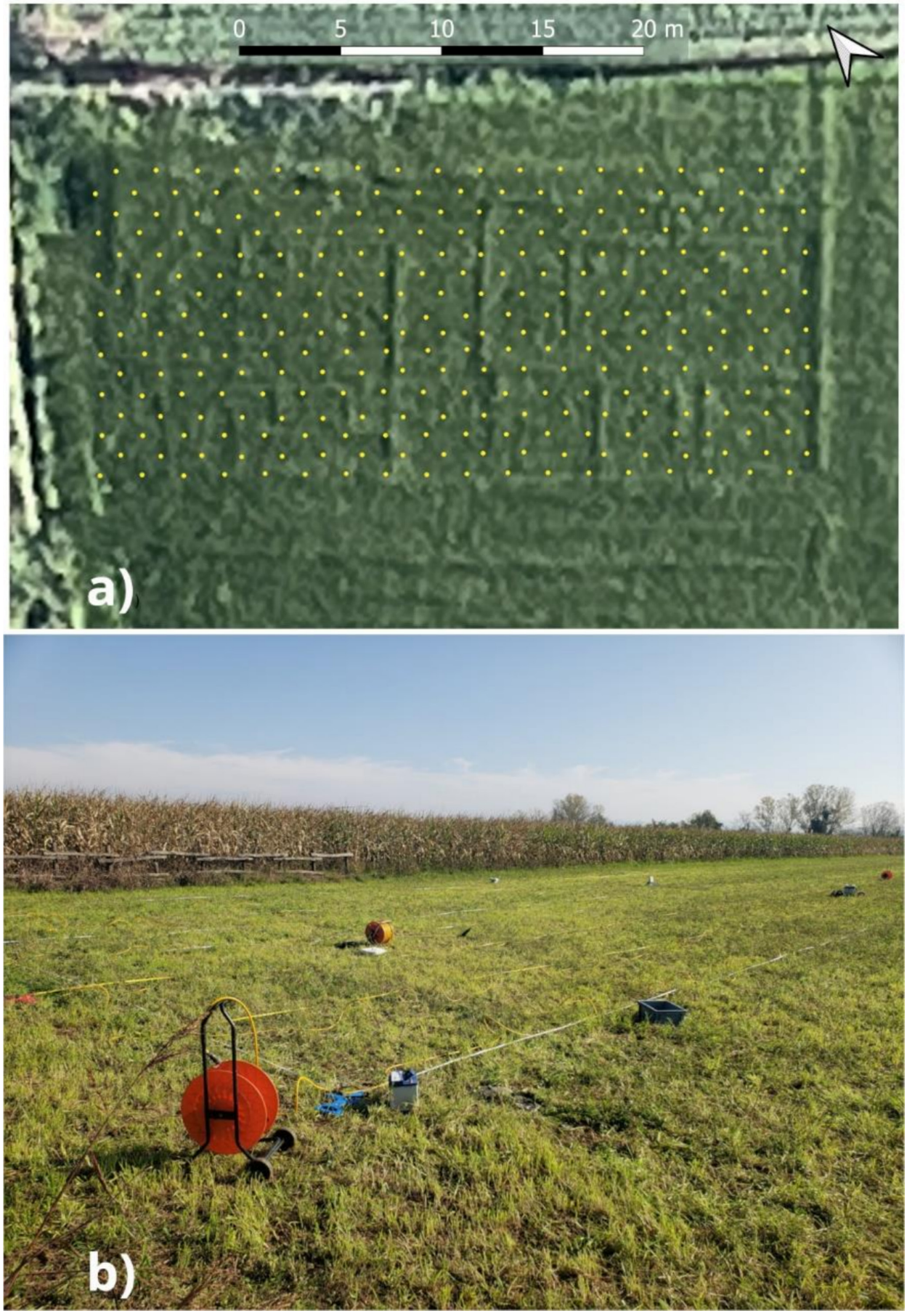


FIGURE 4 | Legend on next page.

10990763, 0, Downloaded from https://onlinelibrary.wiley.com/doi/10.1002/arp.70013 by Politecnico Di Torino Sist. Bibl Del Polit Di Torino, Wiley Online Library on [09/10/2025]. See the Terms and Conditions (https://onlinelibrary.wiley.com/terms-and-conditions) on Wiley Online Library for rules of use; OA articles are governed by the applicable Creative Commons License

FIGURE 4 | Field surveys: (a) Aerial image of the investigated area, acquired from a balloon, showing vegetation stress in correspondence with buried structures (modified from Vergnano et al. 2025). The electrode positions of the ERT survey are shown as yellow dots (Electrode 1 is in the bottom left corner, refer to Figure 3 for electrode numbering); (b) Photo of the ERT survey setup in the investigated area.

volume with very large boundaries. The cells were then converted to points to smooth the effect of the mesh triangulation; the resulting volume was box-clipped and sliced to obtain depth maps, to picture the distribution of electrical resistivity in the subsurface.

2.4 | Comparison Between Full-3D and Quasi-3D Approaches

Whereas the presented full-3D approach consists of measurements with current and dipole electrodes freely distributed on a 2D grid, the quasi-3D approach consists of inverting multiple 2D profiles together. Because the latter has been the most commonly adopted approach in the literature, we compared our full-3D approach to a quasi-3D approach.

Starting from the same dataset acquired, we selected only those measurements where all four electrodes belonged to the same longitudinal line. For example, for the first group of measurements in the top left of Figure 1, we only selected 139, 140, 141 and 142 as potential dipoles (143 and 144 being the current dipoles). In this way, we created a dataset of 1210 measurements, about 75 measurements per each of the 16 lines of 18 electrodes. The so-obtained quadrupoles are mostly dipole–dipole with $a=1$ and $n=1$, 2, 3, and Wenner with $a=1$. We called this subset of the dataset 'longitudinal quasi-3D'. This quasi-3D dataset simulates a survey in which an operator acquires one line at a time and then moves the line and repeats the measurement sequence again and again.

Similarly, we selected only those measurements where all four electrodes belonged to the same transversal line. For example, looking at the second group of measurements in the right part of Figure 1, we only selected 60, 85 and 121 as potential dipoles (49 and 96 being the current dipoles). In this way, we created a dataset of 810 measurements, about 22 measurements for each of the 36 lines of 8 electrodes. We called this subset of the dataset 'transversal quasi-3D'.

The potential difference measurements in the full-3D dataset were not always ordered in a way to directly obtain the potential difference between electrodes on the same line, even if the instrument acquired those measurements simultaneously and with the same current injection. In this case, we summed the potential differences between a certain number of concatenated electrodes until we obtained the potential difference between the two desired electrodes.

Then, we performed the inversion of these two datasets with the same inversion settings and mesh as the full-3D approach. Moreover, we tried to invert also the two quasi-3D datasets together, simulating a survey in which the operator has acquired 2D profiles in both longitudinal and transverse directions, as in a conventional-3D approach.

2.5 | GPR Reference Survey

A multichannel GPR survey was conducted in the same area as the ERT survey. We employed a 600 MHz Stream C system manufactured by IDS, composed of 24 vertically oriented dipoles (VV) and 10 horizontally oriented dipoles (HH). This system therefore contemporarily acquires 32 profiles, spaced about 4 cm (for VV dipoles) and 10 cm (for HH dipoles), with a resulting footprint of about 1 m. The recording time was 100 ns, for a total of 512 samples per trace. Thanks to an odometer, the in-line resolution was set to 4 cm, consistent with the VV off-line resolution. Each trace was georeferenced with an RTK GNSS receiver (Emlid Reach RS2+) with a centimetre accuracy. An operator carried the instrument in parallel acquisition lines spaced about 1 m apart in order to fully cover the survey area with a dense data distribution. Also, the presence of both VV and HH dipoles avoids the necessity of repeating the measurements in two different working directions.

The raw data were processed in ReflexW software (Sandmeier 2021) according to the following processing flow (Vergnano et al. 2025):

1. The running mean over a 4 ns time window was subtracted from each sample, for each trace separately. This is done to reduce instrumental noise that shifts each trace towards positive or negative values. This filter effectively reduces low-frequency noise.
2. Move start-time. The time-zero of each trace was set at the time the receiver antenna registered the direct wave, by using the automatic tool of ReflexW called 'correct max. phase'.
3. Time cut. The signal after 40 ns was deleted because no clear reflections were noted in the radargrams after this time.
4. Background removal. The average trace was subtracted to each trace to attenuate the horizontal clutter along the profiles.
5. Energy decay. A gain function to enhance the weaker reflections at depth.
6. Low pass filter. Frequencies higher than 1000 MHz were cut. Notwithstanding the nominal antenna frequency of 600 MHz, the data showed relevant information in the low-frequency range (i.e., down to about 200 MHz).
7. Subtracting average. The average trace over a trace window of 50 traces (corresponding to about 2.5 m in our acquisition setup) was subtracted from each trace. It is a stronger version of the background removal filter, and is suggested for archaeological applications by Trinks et al. 2018, when the aim of the surveys is the location of wall anomalies (dimensions of about 0.5 m).

10990763, 0, Downloaded from https://onlinelibrary.wiley.com/doi/10.1002/arp.70013 by Politecnico Di Torino Sist. Bibl Del Polit Di Torino, Wiley Online Library on [09/10/2025]. See the Terms and Conditions (https://onlinelibrary.wiley.com/terms-and-conditions) on Wiley Online Library for rules of use; OA articles are governed by the applicable Creative Commons License

8. Normalize profiles. Each of the 32 profiles acquired simultaneously was normalized because some of them naturally acquire a higher amplitude average signal due to instrumental reasons and this effect could bias the visualization of all the profiles together.
9. Median x–y filter. The median of a 2D time-and-trace window of three samples and three traces was calculated for each sample to attenuate scattering effects. Moreover, the initial data volume was denser than necessary given the short spatial (4 cm) and time (0.2 ns) sampling.
10. Stolt migration. The data were migrated with a constant velocity of 0.11 m/ns, retrieved from simple hyperbola fitting. The same velocity was used for time-to-depth conversion.
11. The envelope of the signal was calculated to enhance the visualization of the following processing step:
12. A 3D data volume was created by interpolating all the data in a 3D grid with a pixel size of 5 cm. This data volume was cut into depth slices, which offer optimal visualization for interpretation.

The GPR volume was also exported to Paraview for a 3D interpretation, similar to what was performed on the ERT dataset. The 3D anomalies were extracted through threshold filtering of the reflection intensity scalar field. Additional vertical exaggeration of the GPR volume was applied to emphasize the vertical extension of the reflections. For further information on the GPR and its use in the archaeological site of Augusta Bagiennorum, refer to Vergnano et al. 2025, who performed an extensive GPR survey.

3 | Results

The full-3D inversion converged in seven iterations to a final RMS misfit of 1.17, as reported in the R3.out file in the Supporting Information ('inversions' folder). A selection of relevant depth slices (0.5, 1, 1.5, 2 m below ground level) of the full 3D electrical resistivity model is presented in Figure 5. In Figure 6, a similar selection for GPR slices is also reported. Please note that the Figures in this section are oriented with the North at the top as in the correct geographical location of the test site; therefore, they appear rotated about 50° clockwise compared with the schemes in Section 2 (Figures 1–4).

The resistivity depth slices in Figure 5 reveal the asset of the buried structure, composed of large outer walls, a central inner large wall, several thinner secondary walls and other isolated resistive anomalies, which will be discussed in the next section. The resistivity values range from 40 to about 80 Ωm for the earth infill. Instead, anomalies due to the presence of buried walls show resistive values generally above 150 Ωm. Outer walls reach about 400 Ωm, while inner ones are in the 150–200 Ωm range. The slice at 0.5 m depth (Figure 5a) clearly shows most buried walls. However, the central wall and two isolated and deeper squared anomalies are more visible in the deeper slices.

The reflective areas in the GPR slices, depicted in blue in Figure 6, also display the outer and inner walls of the Roman domus in high detail. The main buried structures are located between 0.5 and 1 m depth, whereas for increasing depths, only the central and outer walls are visible. With respect to the ERT survey, GPR results do not image the central inner wall with the same details (see the comparison between Figure 5c and Figure 6c) as a result of the more limited GPR investigation depth. However, GPR displays the shallower inner walls with more detail than ERT.

An effort was also made to display both ERT and GPR results in 3D in Paraview software, offering another perspective to interpret the data. The 3D visualization of the buried structures detected by ERT and GPR was achieved by tuning the alpha (transparency) channel of the data volume through a manually picked function of the resistivity (and the reflection amplitude for the GPR). 'Resampling to image' Paraview filter solved an issue with the display of the transparent volume and the reference grid. The final result isolates resistive targets (about > 100 Ωm) from the undisturbed soil surrounding them, to appreciate their three-dimensional extension in a single view.

We qualitatively compared the two 3D datasets in Figure 7, yielding some interesting considerations. Firstly, the ERT volume was easier to visualize due to the stark contrast of the resistivity values and very low background noise. Conversely, GPR data display high-frequency noise (isolated spots in Figure 7b), even in a dataset that may be considered very clean. Additionally, the ERT high-resistivity volumetric anomalies are better suited than GPR to display their vertical extension: for this reason, a 2× vertical exaggeration has been applied to the GPR volume, which would otherwise appear almost flat. This effect is related to the different physical principles of the two surveys given that the GPR mainly highlights the surface contrast; for this reason, it is not able to detect the depth extension of the buried structures.

Conversely, the ERT is more able to locate the volumetric extension of high resistivity zones of the model related to the presence of walls. With this respect, the 3D ERT representation better highlights the difference between the main and secondary walls, the former being thicker than the others, whereas in GPR this difference is not similarly clear. Otherwise, for intermediate depths (i.e., 0.5–1 m), the GPR imaging quality is generally better, allowing visualization of an almost perfect planning of the residential building. It has, however, to be underlined that the not perfectly resolved lower right portion of the ERT images (e.g., Figures 5 and 7a) is not related to a limit of the technique but to the misalignment of the survey grids, as already mentioned above with reference to Figure 4a.

4 | Discussion

From the results obtained at the test site, it can be evidenced that, even if the GPR survey appears superior in the identification of a complete plan of the residential building, the 3D ERT survey is still able to reveal most of the geometries detected by GPR. The outline walls of the domus are distinguishable from 0.2 to 2.5 m depth, except for the bottom southwest segment, which could not be resolved due to the positioning of the instrumentation (see Section 2). The inner, thin walls can be identified from 0.3 to 1.0 m depth, appearing most clearly in the 0.5–0.9 m

10990763, 0, Downloaded from https://onlinelibrary.wiley.com/doi/10.1002/arp.70013 by Politecnico Di Torino Sist. Bibl Del Polit Di Torino, Wiley Online Library on [09/10/2025]. See the Terms and Conditions (https://onlinelibrary.wiley.com/terms-and-conditions) on Wiley Online Library for rules of use; OA articles are governed by the applicable Creative Commons License

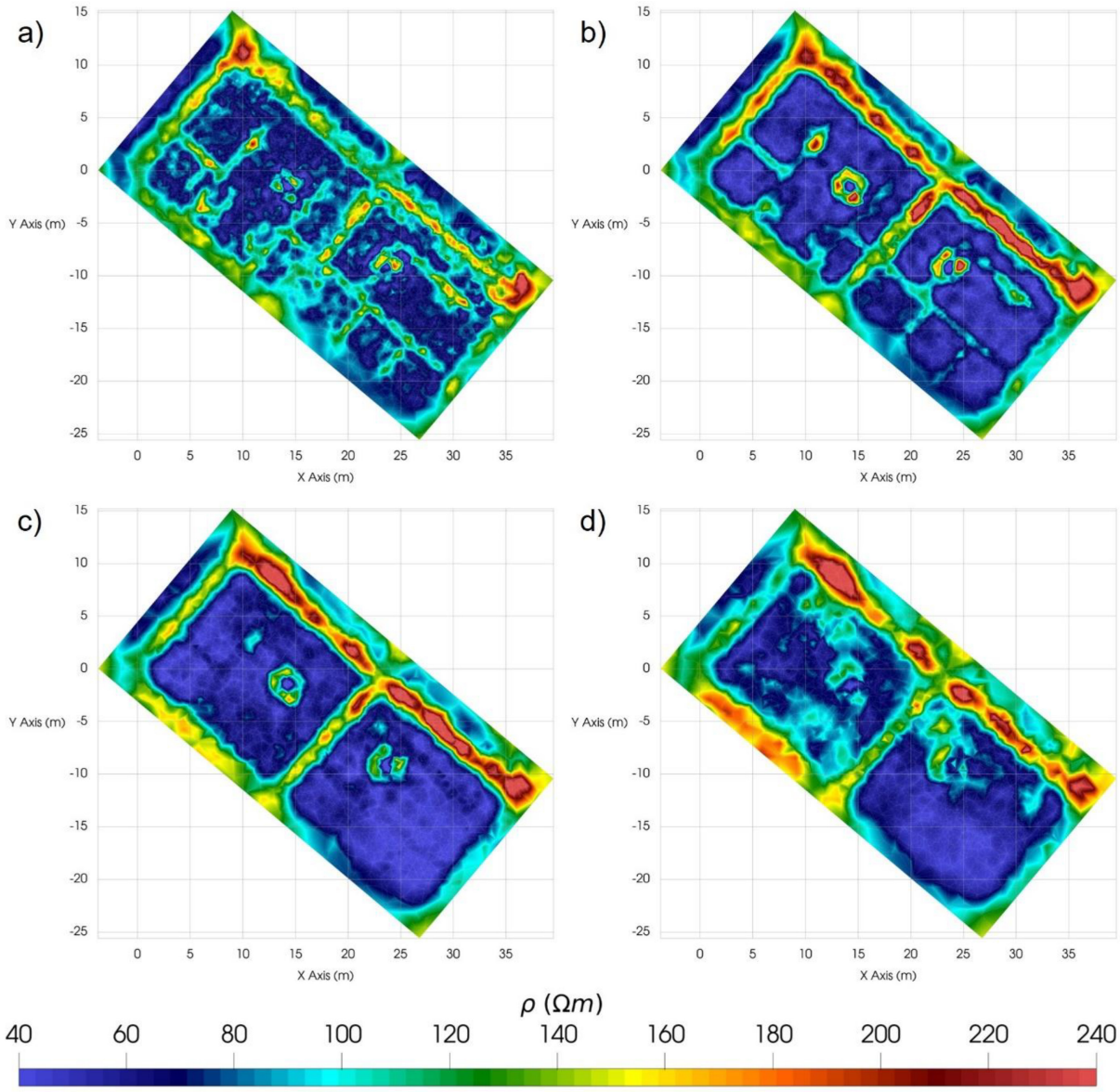


FIGURE 5 | Horizontal slices from the 3D electrical resistivity model at: (a) 0.5 m depth; (b) 1.0 m depth; (c) 1.5 m depth; (d) 2.0 m depth.

depths. To our knowledge, ERT depth slices that display such a clear layout of complex buried archaeological structures have rarely been produced (e.g., Dabas 2008).

In order to better identify the differences and similarities between the ERT and the GPR results, a merging image of the results is proposed in Figure 8 with an overlap of the four depth-slices of ERT and GPR results previously reported. We can observe as the buried walls were identified by the two techniques at the same locations and have the same shapes. This is an important result for the ERT survey, which is generally thought to be not very accurate in shape detection. Moreover, this result was obtained from a survey grid where the electrodes were spaced about 1.4 m between each other, which is a larger distance than the characteristic thickness of the walls (20–50 cm).

However, we also observe that ERT is not very accurate in depicting the depths of the anomalies as the GPR. Scrolling the time slices of the GPR, the data analyst can pinpoint the time, and therefore the depth, at which a buried wall begins to appear. The ERT results are more 'smoothed', and one can see the influence of the buried walls even just below the surface. However, even if not very precise, the ERT is still able to depict the overall 3D shape of buried walls, and probably better than GPR. For example, Figure A4 clarifies that the central wall extends down to about 1.5–2 m depth; below it, there are a pair of metres of conductive sediments, and finally a more resistive geological layer. This information was not possible to retrieve with GPR, whose signal was very attenuated below 1.5 m depth. Therefore, ERT can often be superior in investigation depth compared with GPR, and this can be especially useful in archaeological sites where the sediment layer is thick, or to retrieve geological information other than archaeological information. In this specific survey, the investigation depth was not maximized by the quadrupole sequence used because our focus was to have the best possible resolution near the surface. Because the maximum spacing between electrodes was about 10 m, we can expect to

10990763, 0, Downloaded from https://onlinelibrary.wiley.com/doi/10.1002/arp.70013 by Politecnico Di Torino Sist. Bibl Del Polit Di Torino, Wiley Online Library on [09/10/2025]. See the Terms and Conditions (https://onlinelibrary.wiley.com/terms-and-conditions) on Wiley Online Library for rules of use; OA articles are governed by the applicable Creative Commons License

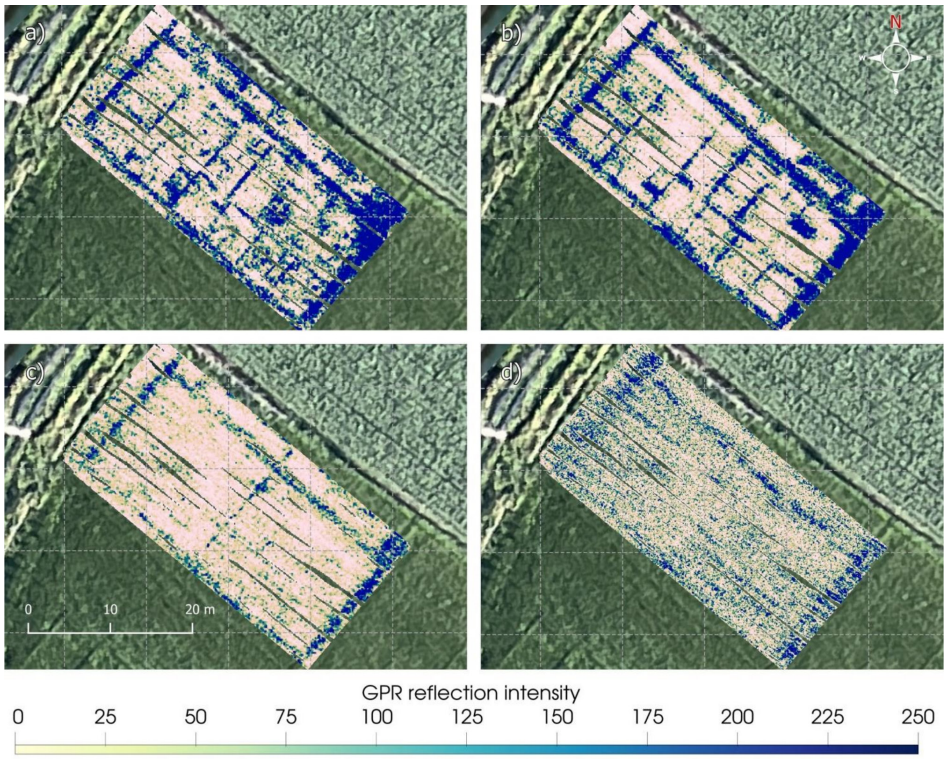


FIGURE 6 | GPR slices at: (a) 0.5 m depth; (b) 1 m depth; (c) 1.5 m depth; (d) 2 m depth. Deeper slices do not show any reflection of interest.

have the most reliable information down to 2–2.5 m of depth, following the known thumb rule that investigation depth is 1/4–1/5 of the electrode spacing. At this depth, we observe a value of about −2 in the sensitivity matrix depicted in Figure A5, which is a soft threshold indicating data reliability (less negative, or positive values. are better), consistently with an observation by Binley (2024). This investigation depth could be easily increased up to 5–6 m (with the same survey grid) by adapting the measurement sequence.

The ERT survey depicted the central wall (circled in green in Figure 8c) as a stronger resistive anomaly than other inner walls, indicating probably its larger thickness or a better conservation state. However, we still advise caution when making considerations about the shape and dimensions of anomalies depicted by ERT, which is not as precise as the GPR in this sense. We observed that, compared with the GPR survey on the same area, the ERT model also displayed two large, squared resistive anomalies (circled in red in Figure 8b). These anomalies strongly contrast with the surrounding subsurface and are markedly visible at 1 m depth (see also Figure 5b). The rightmost resistive anomaly is also detected by GPR, but at a shallower depth (see Figure 8a). These squared anomalies might be hypothesized as well-preserved water tanks or wells, even if direct archaeological evidence is lacking. Another observation is that the main central wall detected by ERT coincides with the central wall detected by GPR at around 1.5 m depth, while the nearby shallower wall detected by GPR is located slightly to the right of it. It seems that ERT is not able to distinguish the two walls correctly, probably because they are very close to each other.

Summarizing, the ERT revealed the disposition of inner and outer walls, the presence of a central larger wall and the two squared anomalies. We investigated the southern side of the *domus*, but it might also develop to the northern side, now occupied by another cultivated field. The precise definition of the planning of the investigated residential building is of archaeological relevance for the test site and specific archaeological excavations are foreseen in this area to gain direct information on the supposed *domus*. Indeed, in the archaeological park of Augusta Bagiennorum, different public areas and buildings were already recognized (e.g., the *forum*, the *basilica* and the *Capitolium*) but, if this structure is confirmed by detailed excavations, this will be the first appearance of a private residential building in the area.

Part of the strategy to increase the lateral survey resolution involved shifting the 2-m-spaced electrode grid after the first acquisition by 1 m right and 1 m up and repeating the acquisition. We conducted a test to understand if such a strategy helped improve the depth-slices representation, as seemed to be the case according to the forward simulations (see Appendix A). Figure 9 compares a 0.7-m-depth slice of the resistivity model obtained using the entire dataset (dense coverage of electrodes) and the same depth slice obtained using half of the dataset, i.e., just the first of the two acquisitions (coarse coverage of electrodes). The mesh and other inversion parameters were the same in both inversions. We observe that the outer and inner walls are clearly distinguishable in both images. However, the smaller anomalies, such as the two squared anomalies symmetrical with respect to the central wall, are better defined in the results of the inversion with the dense dataset with respect to that of the coarse dataset.

The adopted survey strategy increased the resolution from a 2-m-spaced electrode grid to a 1.4-m-spaced electrode grid in a very convenient way, logistically speaking.

10990763, 0, Downloaded from https://onlinelibrary.wiley.com/doi/10.1002/arp.70013 by Politecnico Di Torino Sist. Bibl Del Polit Di Torino, Wiley Online Library on [09/10/2025]. See the Terms and Conditions (https://onlinelibrary.wiley.com/terms-and-conditions) on Wiley Online Library for rules of use; OA articles are governed by the applicable Creative Commons License

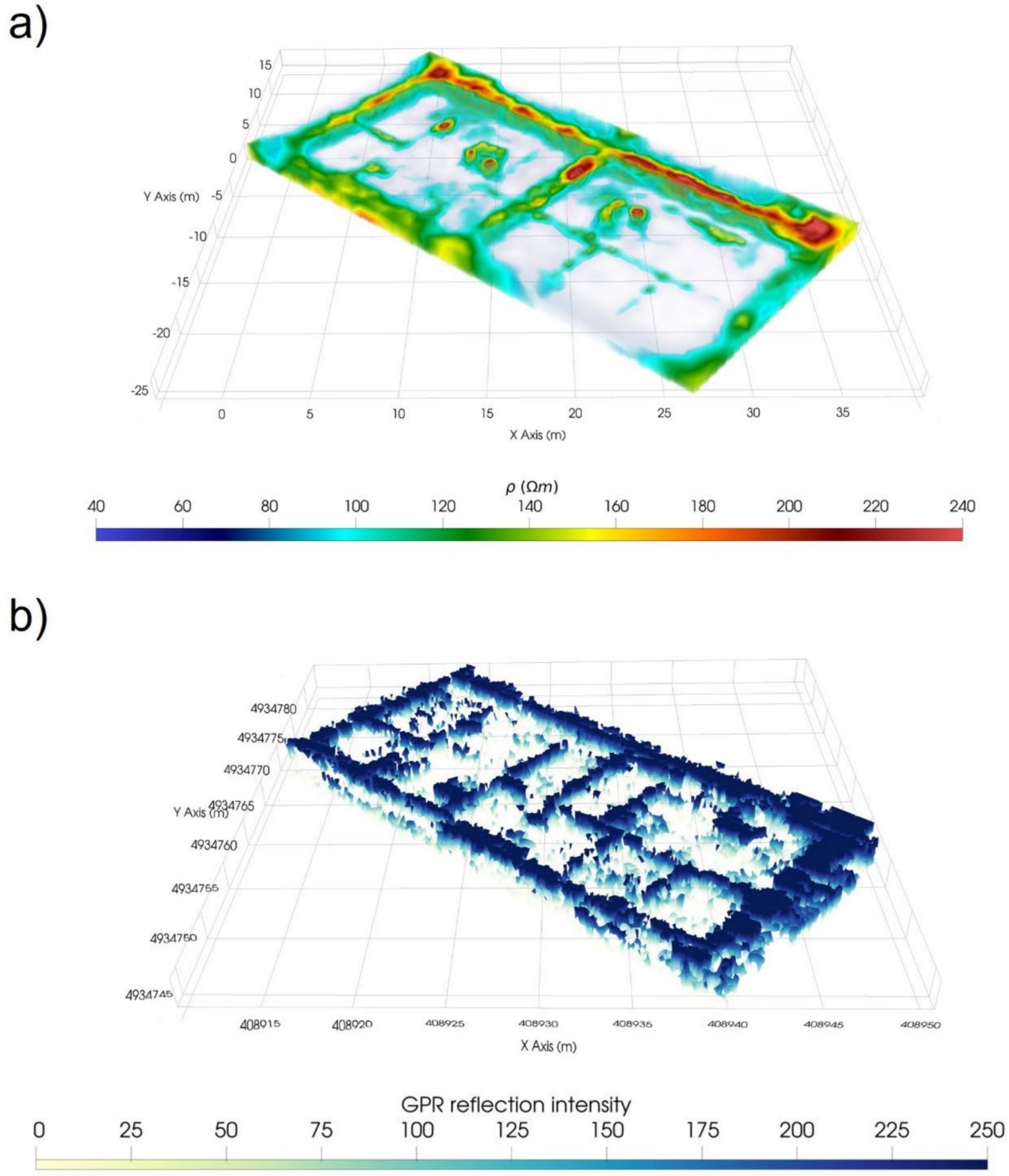


FIGURE 7 | (a) The resistive anomalies contained in a subset of the 3D ERT volume (depths between 0.5 and 2.0 m). (b) The GPR anomalies are displayed based on the reflection intensity. A 2× vertical exaggeration has been applied to the GPR data to facilitate the visualization.

For future surveys on similar sites, if a preliminary screening is needed, one could start with a 3- or 4-m spaced electrode grid to rapidly cover a wider area. A second, more detailed survey with electrodes spaced 1 or 2 m can then be performed in specific areas of interest. In both preliminary and detailed surveys, we suggest this approach: to begin with a certain electrode grid and then increase the lateral resolution by shifting the grid by half of the electrode spacing in both the x and y directions.

10990763, 0, Downloaded from https://onlinelibrary.wiley.com/doi/10.1002/arp.70013 by Politecnico Di Torino Sist. Bibl Del Polit Di Torino, Wiley Online Library on [09/10/2025]. See the Terms and Conditions (https://onlinelibrary.wiley.com/terms-and-conditions) on Wiley Online Library for rules of use; OA articles are governed by the applicable Creative Commons License

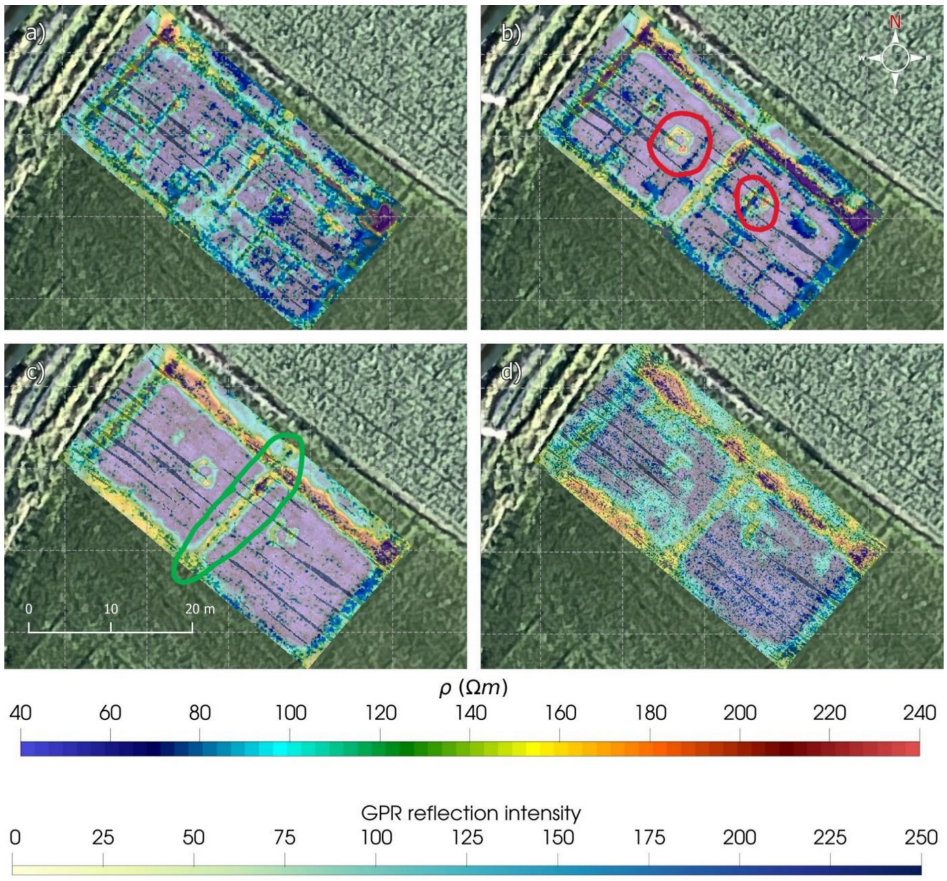


FIGURE 8 | Comparison view of ERT and GPR depth-slices at several depths: (a) 0.5 m depth, (b) 1 m depth, (c) 1.5 m depth, (d) 2 m depth. The depth-slices were overlapped and the ERT ones were made semi-transparent. Two large, squared resistive anomalies and the central wall depicted by ERT are also evidenced with red circles in (b) and green circle in (c), respectively.

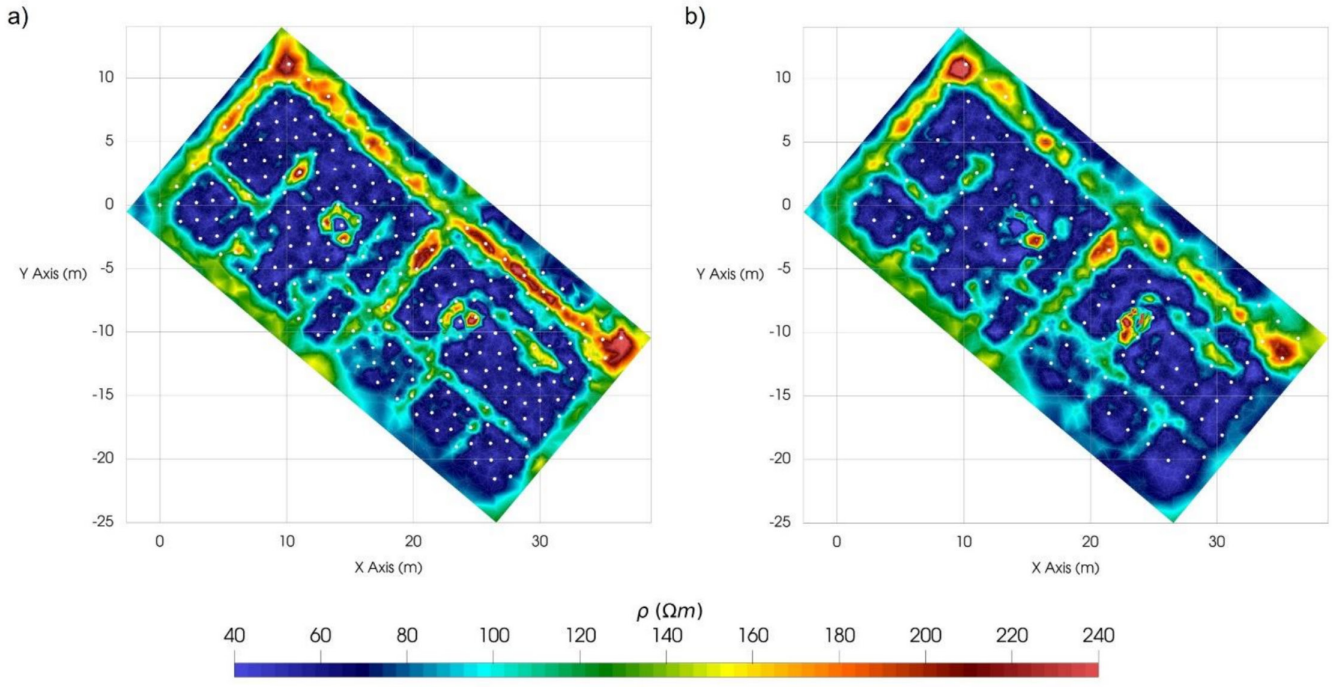


FIGURE 9 | A comparison of the results of 3D ERT inversion from the (a) dense dataset and (b) coarse dataset. Both setups manage to resolve the outer and inner walls of the domus, but with the dense setup, the anomalies can be distinguished more clearly than the coarse setup.

10990763, 0, Downloaded from https://onlinelibrary.wiley.com/doi/10.1002/arp.70013 by Politecnico Di Torino Sist. Bibl Del Polit Di Torino, Wiley Online Library on [09/10/2025]. See the Terms and Conditions (https://onlinelibrary.wiley.com/terms-and-conditions) on Wiley Online Library for rules of use; OA articles are governed by the applicable Creative Commons License

Thanks to the ERT acquisition sequence developed within this study, we were able to perform each 3D ERT acquisition of 9940 measurements within 40 min. The total time needed to set up the two surveys and dismantle the instruments was less than 4 h. The GPR dataset was conversely acquired in about 2 h, half of the time necessary for the ERT survey.

The sequence management program is open-source and reusable for future full-3D archaeological ERT surveys. It has the advantages of:

- being adaptable to different grid setups (the x and y dimensions of the grid are input parameters);
- allowing us to perform a high-speed acquisition with ERT instruments able to acquire 10 measurements at a time (which are common, commercially);
- being focused for archaeological investigations in terms of investigation depth and sensitivity to shallow buried structures but customizable to reach greater investigation depths;
- being safe from polarization errors in measurements.

In past research, the ERT has seldom been used with a full-3D approach in archaeology. However, quasi-3D ERT results can be subject to sensitivity errors of each section and are especially sensitive to the direction of acquisition. Sometimes, misleading results have been reported when performing 2D acquisitions on a site with substructures better described in a 3D environment (Bentley and Gharibi 2004). The presence of 3D inversion artefacts based on the direction of the 2D lines has also been already addressed in several publications (e.g., N. G. Papadopoulos et al. 2006, 2007, 2010, 2011; Berge and Drahor 2011a, 2011b). When working with 2D lines, a conventional-3D ERT should be employed instead of the quasi-3D approach, acquiring profiles in both the x and y directions to reduce the directional bias, but this doubles the investigation time (Loke 2004).

To estimate the difference between a full-3D and a quasi- or conventional-3D survey on the same site, we created a subset of our dataset with only measurements in which all four electrodes belonged to the same longitudinal line ('longitudinal quasi-3D'), transversal line ('transversal quasi-3D'), and a combination of the two ('conventional 3D'). In these comparisons, all the potentially available acquisition lines are considered, including the ones with the shifted electrodes and with the potentially higher resolution. Figure 10 shows the results of this comparison.

In Figure 10a, the longitudinal quasi-3D approach detects the northern main wall and the central wall, and the positions of secondary walls are slightly highlighted as resistive anomalies, though not precisely. In Figure 10b, instead, the eastern wall is depicted, but the northern wall is almost absent. Interestingly, the two squared anomalies, clearly depicted in the full-3D approach (Figure 10d), are 'seen' by the quasi-3D as just two resistive point anomalies oriented in the same direction as the quasi-3D survey. Inverting the two quasi-3D datasets together leads to a clearer result (Figure 10c), in which all the anomalies are depicted, even with lower quality than the full-3D. Moreover, the acquisition time of a full-3D survey is lower than the sum of the acquisition times of multiple parallel ERT profiles reaching a similar resolution.

Clearly, the quality of the comparisons presented is affected by the number of acquisitions considered in the longitudinal and transversal datasets. In our analyses, these data were extracted from the full 3D dataset, while a specific acquisition, calibrated in the aim of a conventional 3D approach, would potentially result in an increased number of measurements along each line (depending on the chosen dipoles and survey specifications). However, in our opinion, the spatial distribution of the measurements has more relevance with respect to their total number: In conventional 3D, the absence of cross-line measurements strongly limits the transversal resolution and the imaging of lateral structures, and this could not be changed even by increasing the number of inline measurements.

These observations confirm the hypothesis that quasi-3D approaches can highlight different anomalies based on which direction the survey is carried out and are, therefore, not completely trustworthy, especially in archaeological investigations where anomalies of complex shapes can be present. The full-3D approach represents, according to the results of this study (see also Appendix A in this respect), the best option to acquire the most reliable data, with survey times similar to those of a quasi-3D approach.

Acquisition times and costs of ERT surveys are still significantly higher than other usually adopted prospection methods in archaeology (i.e., GPR and Geomagnetic surveys). In this respect, the ERT surveys cannot be seen as a fully adequate alternative to these methodologies, particularly when the areas to be investigated are wide, unless one can reduce acquisition times using an automatic system such as the ARP (Dabas 2008). However, in specific locations where a more detailed representation of specific anomalies is necessary, or in challenging subsoil conditions for the other methodologies, the ERT surveys are an interesting alternative approach. Although this methodology may not be considered as fast as the GPR, the quality of its results is appealing. In the specific case study, the GPR granted some clear results due to the especially suitable ground conditions. This may not be the case in other scenarios, such as bumped terrain or clayey deposits, which severely limit the depth of GPR measurements (Jol and Bristow 2003; Leckebusch 2003; De Domenico et al. 2006; Comina et al. 2025). In such cases, the full-3D ERT survey is a valid alternative to explore archaeological sites of interest that are difficult to investigate with GPR.

ERT and GPR can also be complementary, provided that one has the resources to survey an archaeological area with both techniques. GPR still has the advantage of pinpointing the location of small, buried structures, but ERT can sometimes display anomalies that GPR is not sensitive to due to the different physical properties involved. GPR still has a distinctive advantage over ERT in estimating the depth of the buried structures, provided that one can estimate the velocity of electromagnetic waves in the subsoil, but often reaches lower maximum investigation depth than ERT.

10990763, 0, Downloaded from https://onlinelibrary.wiley.com/doi/10.1002/arp.70013 by Politecnico Di Torino Sist. Bibl Del Polit Di Torino, Wiley Online Library on [09/10/2025]. See the Terms and Conditions (https://onlinelibrary.wiley.com/terms-and-conditions) on Wiley Online Library for rules of use; OA articles are governed by the applicable Creative Commons License

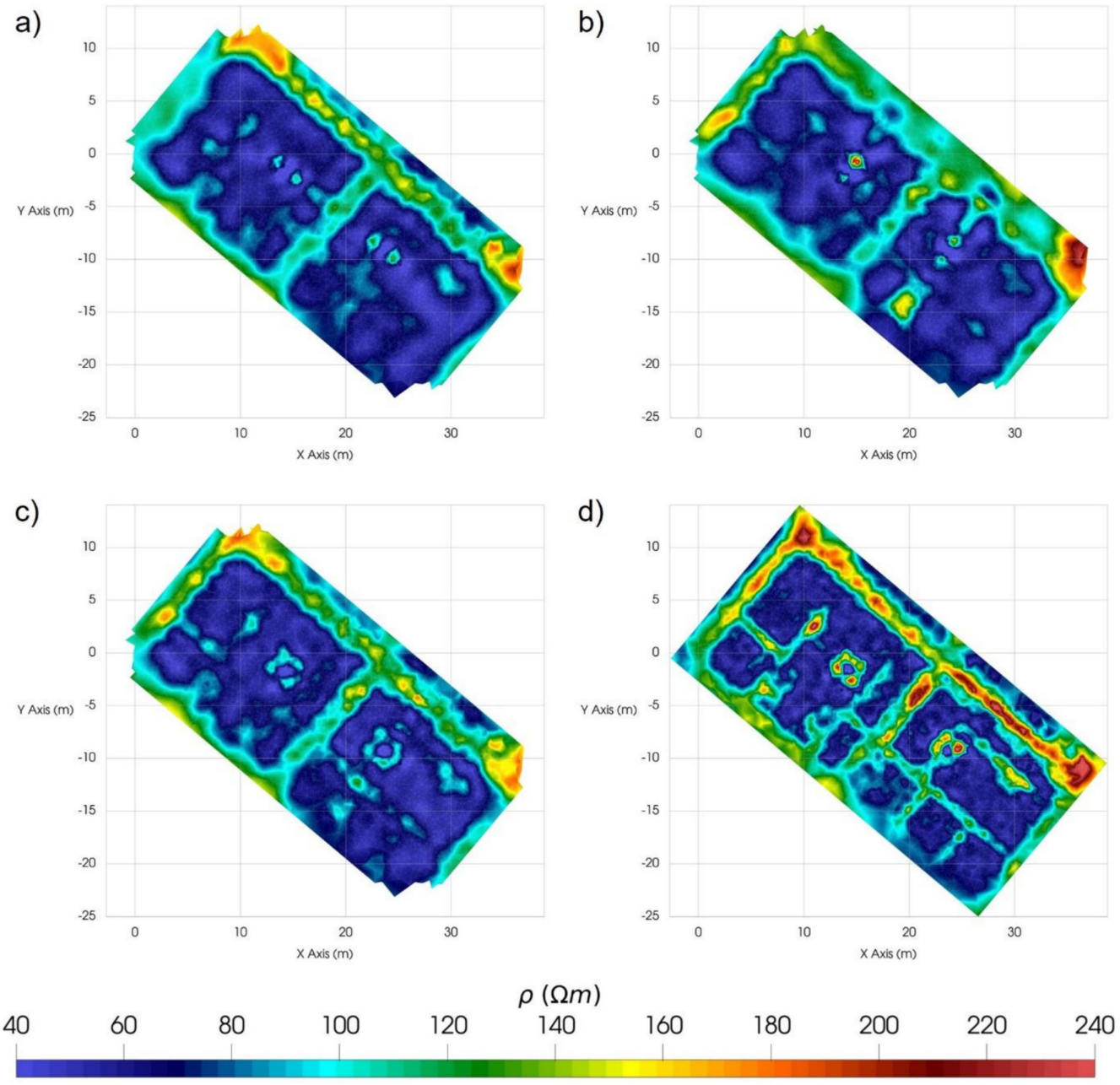


FIGURE 10 | ERT depth slices at 0.7 m depth using (a) longitudinal quasi-3D approach (total inverted data: 1210; final RMS misfit: 0.91), (b) transversal quasi-3D approach (total inverted data: 810; final RMS misfit: 1.00), (c) longitudinal and transversal datasets together (total inverted data: 2020; final RMS misfit: 1.11), (d) full-3D approach (total inverted data: 19 880; final RMS misfit: 1.17).

5 | Conclusion

This study explored a full-3D ERT acquisition for shallow archaeological prospection, using 144 electrodes as both current and potential electrodes in an 18×8 electrode grid. We wrote an open-source computer code to build fast and reliable 3D ERT quadrupole sequences specific for archaeological purposes. The survey strategy involved shifting the electrode grid by half of the electrode spacing in both the longitudinal and transversal directions and repeating the measurement a second time to increase the resolution.

The main outcome of the resistivity models is identifying the outer and inner walls of a well-preserved Roman *domus*. The results showed the capabilities of the full-3D ERT inversion of dense 3D data to locate buried structures with an accuracy comparable to that of a multichannel GPR survey. Moreover, the ERT revealed two squared anomalies that the GPR could not display clearly and revealed that, among the inner walls of the buried structure, the central wall is thicker. The results suggest that a full-3D ERT survey is sensitive to anomalies that develop in different directions: The walls reconstructed by our inversion of full-3D data are clearly characterized both in the longitudinal and transverse directions, whereas a test of the quasi-3D approach revealed significant directional bias. These findings indicate that full-3D ERT surveys are a valid and flexible alternative to the GPR surveys for archaeological prospections, especially in sites with challenging terrain

10990763, 0, Downloaded from https://onlinelibrary.wiley.com/doi/10.1002/arp.70013 by Politecnico Di Torino Sist. Bibl Del Polit Di Torino, Wiley Online Library on [09/10/2025]. See the Terms and Conditions (https://onlinelibrary.wiley.com/terms-and-conditions) on Wiley Online Library for rules of use; OA articles are governed by the applicable Creative Commons License

conditions, provided that dense data coverage and accurate inversion modelling are accomplished.

This evidence is, at the moment, limited to the results obtained at the specific test site reported in the paper, and further surveys are necessary to completely confirm the potentiality of the method. Future research could explore the full-3D ERT in other archaeological sites, to test if the outcomes of this study can be generally valid or they are site-dependent. In particular, it would be interesting to test this approach on archaeological sites where other techniques such as GPR did not give clear results. Also, thanks to the flexibility of the ERT technique and the sequence generator, archaeological sites with buried remains located deeper than the usual 1–2 m investigated by GPR, or with stratified layers, could also be explored. However, we did not test deeper investigations, which could easily face resolution issues.

The comparison between GPR and ERT is particularly important when planning to build in a potentially archaeological area. Generally, the presence of buried structures in construction sites is preliminarily assessed by GPR. However, if the soil has some clay content, GPR may not properly detect buried structures due to its limited penetration depth. Therefore, a wider knowledge of alternative techniques such as full-3D ERT could be beneficial to bring them to wider use among professionals.

Acknowledgements

We thank Francesco Tozzato and Han Yan for their precious help during fieldwork. We thank Servizio di Posizionamento Interregionale GNSS (SPIN3 GNSS, https://www.spingnss.it/) for the RTK corrections that improved the georeferencing accuracy of our GNSS receiver. The research activity of F. Pace is funded by the NOP Research and Innovation 2014–2020, Axis IV 'Education and research for recovery –REACT-EU'. Authors are indebted to the Applied Geophysics Laboratory of the Department of Environment, Land and Infrastructure Engineering at Polytechnic of Turin for the availability of ERT instrumentation. Open access publishing facilitated by Universita degli Studi di Torino, as part of the Wiley - CRUI-CARE agreement.

Conflicts of Interest

The authors declare no conflicts of interest.

Data Availability Statement

The authors promote the reuse, implementation and modification of any code, data and method reported in this paper. In the Supporting Information, you can find the following files:

- Raw and filtered ERT data
- Raw and processed GPR data
- ERT (full 3D and quasi 3D) inversion results
- R script to write the full-3D ERT sequence
- Fortran script to reorder the sequence to avoid using an electrode as a potential electrode just after being used as a current electrode
- R script to extract the quasi-3D dataset from the full-3D dataset

Please see more details in the readme.txt file of the Supporting Information. The computer codes can also be found in a public repository at https://github.com/Andrea-Vergnano/geophysics-utils, in which the authors will post updated versions, and comments can be made in order to improve them.

References

Abdullah, F. M., M. H. Loke, M. Nawawi, and K. Abdullah. 2019. "Improving the Resolution of 3-D Resistivity Surveys Along the Perimeter of a Confined Area Using Optimized Arrays." *Pure and Applied Geophysics* 176, no. 4: 1701–1715.

Al Hagrey, S. A. 2012. "2D Optimized Electrode Arrays for Borehole Resistivity Tomography and CO2 Sequestration Modelling." *Pure and Applied Geophysics* 169: 1283–1292. https://doi.org/10.1007/s00024-011-0369-0.

Al-Saadi, O. S., V. Schmidt, M. Becken, and T. Fritsch. 2018. "Very-High-Resolution Electrical Resistivity Imaging of Buried Foundations of a Roman Villa Near Nonnweiler, Germany." *Archaeological Prospection* 25: 209–218. https://doi.org/10.1002/arp.1703.

Argote-Espino, D., A. Tejero-Andrade, G. Cifuentes-Nava, et al. 2013. "3D Electrical Prospection in the Archaeological Site of El Pahñú, Hidalgo State, Central Mexico." *Journal of Archaeological Science* 40: 1213–1223. https://doi.org/10.1016/j.jas.2012.08.034.

Argote-Espino, D. L., P. A. López-García, and A. Tejero-Andrade. 2016. "3D-ERT Geophysical Prospecting for the Investigation of Two Terraces of an Archaeological Site Northeast of Tlaxcala State, Mexico." *Journal of Archaeological Science: Reports* 8: 406–415. https://doi.org/10.1016/j.jasrep.2016.06.047.

Arosio, D., A. Hojat, V. I. Ivanov, et al. 2018. "A Laboratory Experience to Assess the 3D Effects on 2D ERT Monitoring of River Levees, in: 24th European Meeting of Environmental and Engineering Geophysics." In *Presented at the 24th European Meeting of Environmental and Engineering Geophysics, European Association of Geoscientists & Engineers, Porto, Portugal*, 1–5. https://doi.org/10.3997/2214-4609.201802628.

Assandria, G., and G. Vacchetta. 1925. *Augusta Bagiennorum: Planimetria Generale Degli Scavi con Cenni Illustrativi*. Tipografia Francesco Vissio.

Bentley, L. R., and M. Gharibi. 2004. "Two- and Three-Dimensional Electrical Resistivity Imaging at a Heterogeneous Remediation Site." *Geophysics* 69: 674–680. https://doi.org/10.1190/1.1759453.

Berge, M. A., and M. G. Drahor. 2011a. "Electrical Resistivity Tomography Investigations of Multilayered Archaeological Settlements: Part I—Modelling." *Archaeological Prospection* 18, no. 3: 159–171.

Berge, M. A., and M. G. Drahor. 2011b. "Electrical Resistivity Tomography Investigations of Multilayered Archaeological Settlements: Part II—A Case From Old Smyrna Hoyuk, Turkey." *Archaeological Prospection* 18, no. 4: 291–302.

Bièvre, G., L. Oxarango, T. Günther, D. Goutaland, and M. Massardi. 2018. "Improvement of 2D ERT Measurements Conducted Along a Small Earth-Filled Dyke Using 3D Topographic Data and 3D Computation of Geometric Factors." *Journal of Applied Geophysics* 153: 100–112. https://doi.org/10.1016/j.jappgeo.2018.04.012.

Binley, A. 2024. "R3t User Guide." 26 pp. http://www.es.lancs.ac.uk/people/amb/Freeware/R3t/R3t_readme.pdf.

Binley, A., and A. Kemna. 2005. "Electrical Methods." In *Hydrogeophysics* by, edited by Y. Rubin and S. S. Hubbard, 129–156. Springer.

Blanchy, G., S. Saneiyan, J. Boyd, P. McLachlan, and A. Binley. 2020. "ResIPy, an Intuitive Open Source Software for Complex Geoelectrical Inversion/Modeling." *Computers & Geosciences* 137: 104423. https://doi.org/10.1016/j.cageo.2020.104423.

Boyd, J., G. Blanchy, S. Saneiyan, P. Mclachlan, and A. Binley. 2019. "3D Geoelectrical Problems With ResiPy, an Open Source Graphical User Interface for Geoelectrical Data Processing." *Fast Times* 24, no. 4: 85–92. https://doi.org/10.13140/RG.2.2.35381.63205.

Capizzi, P., R. Martorana, P. Messina, and P. L. Cosentino. 2012. "Geophysical and Geotechnical Investigations to Support the Restoration Project of the Roman 'Villa del Casale', Piazza Armerina,

10990763, 0, Downloaded from https://onlinelibrary.wiley.com/doi/10.1002/arp.70013 by Politecnico Di Torino Sist. Bibl Del Polit Di Torino, Wiley Online Library on [09/10/2025]. See the Terms and Conditions (https://onlinelibrary.wiley.com/terms-and-conditions) on Wiley Online Library for rules of use; OA articles are governed by the applicable Creative Commons License

Sicily, Italy." *Near Surface Geophysics* 10: 145–160. https://doi.org/10.3997/1873-0604.2011038.

Casas, A., P. L. Cosentino, G. Fiandaca, et al. 2018. "Non-Invasive Geophysical Surveys in Search of the Roman Temple of Augustus Under the Cathedral of Tarragona (Catalonia, Spain): A Case Study." *Surveys in Geophysics* 39: 1107–1124. https://doi.org/10.1007/s10712-018-9470-6.

Chávez, R. E., A. Tejero-Andrade, G. Cifuentes, D. L. Argote-Espino, and E. Hernández-Quintero. 2018. "Karst Detection Beneath the Pyramid of El Castillo, Chichen Itza, Mexico, by Non-Invasive ERT-3D Methods." *Scientific Reports* 8: 15391. https://doi.org/10.1038/s41598-018-33888-9.

Clark, A. 1996. *Seeing Beneath the Soil: Prospecting Methods in Archaeology*. Batsford.

Colombero, C., C. Comina, D. Rocchietti, G. B. Garbarino, and L. Sambuelli. 2021. "Ground Penetrating Radar Surveys in the Archaeological Area of *Augusta Bagiennorum*: Comparisons Between Geophysical and Archaeological Campaigns." *Archaeological Prospection* 29: arp.1855. https://doi.org/10.1002/arp.1855.

Comina, C., R. Leone, I. Palmisano, and A. Vergnano. 2025. "Off-Line Stacking for Multichannel GPR Processing in Clay-Rich Archaeological Sites: The Case Study of Tindari (Sicily)." *Applied Sciences* 15: 7157. https://doi.org/10.3390/app15137157.

Conyers, L. B. 2018. "Ground-Penetrating Radar." In *Ground-Penetrating Radar and Magnetometry for Buried Landscape Analysis*. SpringerBriefs in Geography. Springer. https://doi.org/10.1007/978-3-319-70890-4_2.

Dabas, M. 2008. "Theory and Practice of the New Fast Electrical Imaging System ARP." In *Seeing the Unseen—Geo-Physics and Landscape Archaeology*, 105–126. CRC Press.

David, A., N. Linford, P. Linford, L. Martin, and A. Payne. 2008. *Geophysical Survey in Archaeological Field Evaluation*. 2nd ed. English Heritage.

De Domenico, D., F. Giannino, G. Leucci, and C. Bottari. 2006. "Integrated Geophysical Surveys at the Archaeological Site of Tindari (Sicily, Italy)." *Journal of Archaeological Science* 33: 961–970. https://doi.org/10.1016/j.jas.2005.11.004.

Fernández-Álvarez, J.-P., D. Rubio-Melendi, J. A. Quirós Castillo, A. González-Quirós, and D. Cimadevilla-Fuente. 2017. "Combined GPR and ERT Exploratory Geophysical Survey of the Medieval Village of Pancorbo Castle (Burgos, Spain)." *Journal of Applied Geophysics* 144: 86–93. https://doi.org/10.1016/j.jappgeo.2017.07.002.

Fiandaca, G., P. L. Cosentino, R. Martorana, and P. Messina. 2010. "The MYG Methodology to Carry Out 3D Electrical Resistivitytomography on Media Covered by Vulnerable Surfaces of Artistic Value." *Il Nuovo Cimento B* 125: 711–718. https://doi.org/10.1393/ncb/i2010-10885-3.

Fischanger, F., G. Morelli, D. LaBrecque, and M. Occhi. 2007. "Monitoring Resins Injection With 3D Electrical Resistivity Tomography (ERT) Using Surface and Multi-Borehole Electrode Arrays." In *Presented at the Symposium on the Application of Geophysics to Engineering and Environmental Problems 2007, Environment and Engineering Geophysical Society*, 1226–1233. https://doi.org/10.4133/1.2924630.

Furman, A., T. P. Ferré, and G. L. Heath. 2007. "Spatial Focusing of Electrical Resistivity Surveys Considering Geologic and Hydrologic Layering." *Geophysics* 72: F65–F73. https://doi.org/10.1190/1.2433737.

Gaber, A., K. S. Gemail, A. Kamel, H. M. Atia, and A. Ibrahim. 2021. "Integration of 2D/3D Ground Penetrating Radar and Electrical Resistivity Tomography Surveys as Enhanced Imaging of Archaeological Ruins: A Case Study in San El-Hager (Tanis) Site, Northeastern Nile Delta, Egypt." *Archaeological Prospection* 28: 251–267. https://doi.org/10.1002/arp.1810.

García-Nieto, M. C., M. A. Martínez-Segura, M. Navarro, I. Valverde-Palacios, and P. Martínez-Pagán. 2024. "A Geophysical Investigation in Which 3D Electrical Resistivity Tomography and Ground-Penetrating Radar Are Used to Determine Singularities in the Foundations of the Protected Historic Tower of Murcia Cathedral (Spain)." *Remote Sensing* 16, no. 21: 4117.

Geuzaine, C., and J. Remacle. 2009. "Gmsh: A 3-D Finite Element Mesh Generator With Built-In Pre- and Post-Processing Facilities." *International Journal for Numerical Methods in Engineering* 79: 1309–1331. https://doi.org/10.1002/nme.2579.

Hansen, C. D., and C. R. Johnson. 2005. "ParaView: An End-User Tool for Large Data Visualization." In *The Visualisation Handbook*. Elsevier-Butterworth Heinemann.

Hojat, A. 2024. "An Iterative 3D Correction Plus 2D Inversion Procedure to Remove 3D Effects From 2D ERT Data Along Embankments." *Sensors* 24: 3759. https://doi.org/10.3390/s24123759.

Hojat, A., D. Arosio, V. I. Ivanov, et al. 2020. "Quantifying Seasonal 3D Effects for A Permanent Electrical Resistivity Tomography Monitoring System Along the Embankment of an Irrigation Canal." *Near Surface Geophysics* 18: 427–443. https://doi.org/10.1002/nsg.12110.

Hung, Y.-C., C.-P. Lin, C.-T. Lee, and K.-W. Weng. 2019. "3D and Boundary Effects on 2D Electrical Resistivity Tomography." *Applied Sciences* 9: 2963. https://doi.org/10.3390/app9152963.

Iris Instruments. 2024. "Prosys III".

Jol, H. M., and C. S. Bristow. 2003. "GPR in Sediments: Advice on Data Collection, Basic Processing and Interpretation, A Good Practice Guide." *SP* 211: 9–27. https://doi.org/10.1144/GSL.SP.2001.211.01.02.

Karaoulis, M., G. Tsokas, P. Tsourlos, P. Bogiatzis, and G. Vargemezis. 2025. "3D Electrical Resistivity Tomography Using a Radial Array and Detailed Topography for Tumuli Prospection." *Archaeological Prospection* 32: 197–208.

Leckebusch, J. 2003. "Ground-Penetrating Radar: A Modern Three-Dimensional Prospection Method." *Archaeological Prospection* 10: 213–240. https://doi.org/10.1002/arp.211.

Leucci, G., and F. Greco. 2012. "3D ERT Survey to Reconstruct Archaeological Features in the Subsoil of the "Spirito Santo" Church Ruins at the Site of Occhiolà (Sicily, Italy)." *Archaeology* 1: 1–6.

Linford, N. 2006. "The Application of Geophysical Methods to Archaeological Prospection." *Reports on Progress in Physics* 69: 2205–2257. https://doi.org/10.1088/0034-4885/69/7/R04.

Loke, M. H. 2004. "Tutorial: 2-D and 3-D Electrical Imaging Surveys." 136 pp. https://sites.ualberta.ca/~unsworth/UA-classes/223/loke_course_notes.pdf.

Loke, M. H., J. E. Chambers, D. F. Rucker, O. Kuras, and P. B. Wilkinson. 2013. "Recent Developments in the Direct-Current Geoelectrical Imaging Method." *Journal of Applied Geophysics* 95: 135–156.

Loke, M. H., N. Papadopoulos, P. B. Wilkinson, D. Oikonomou, K. Simyrdanis, and D. F. Rucker. 2020. "The Inversion of Data From Very Large Three-Dimensional Electrical Resistivity Tomography Mobile Surveys." *Geophysical Prospecting* 68: 2579–2597.

Loke, M. H., P. B. Wilkinson, S. S. Uhlemann, J. E. Chambers, and L. S. Oxby. 2014. "Computation of Optimized Arrays for 3-D Electrical Imaging Surveys." *Geophysical Journal International* 199, no. 3: 1751–1764.

Louvaris, P., P. Tsourlos, G. Vargemezis, and G. Tsokas. 2025. "Three-Dimensional Electrical Resistivity Tomography Schemes Optimized for Imaging Wall Foundations." *Archaeological Prospection* 32, no. 3: 726–739. https://doi.org/10.1002/arp.1991.

Lu, E., E. Erkul, S. Fischer, M. Gräber, and W. Rabbel. 2023. "Application of 3D ERT and GPR in Modern Archaeology – an Example for Mapping New-Age Urban Remains." In *Advances In on- and Offshore*

10990763, 0, Downloaded from https://onlinelibrary.wiley.com/doi/10.1002/arp.70013 by Politecnico Di Torino Sist. Bibl Del Polit Di Torino, Wiley Online Library on [09/10/2025]. See the Terms and Conditions (https://onlinelibrary.wiley.com/terms-and-conditions) on Wiley Online Library for rules of use; OA articles are governed by the applicable Creative Commons License

Archaeological Prospection: Proceedings of the 15th International Conference on Archaeological Prospection. Universitätsverlag Kiel. https://doi.org/10.38072/978-3-928794-83-1/p74.

Martorana, R., P. Capizzi, A. D'Alessandro, and D. Luzio. 2017. "Comparison of Different Sets of Array Configurations for Multichannel 2D ERT Acquisition." *Journal of Applied Geophysics* 137: 34–48. https://doi.org/10.1016/j.jappgeo.2016.12.012.

Negri, S., G. Leucci, and F. Mazzone. 2008. "High Resolution 3D ERT to Help GPR Data Interpretation for Researching Archaeological Items in a Geologically Complex Subsurface." *Journal of Applied Geophysics* 65: 111–120. https://doi.org/10.1016/j.jappgeo.2008.06.004.

Papadopoulos, N., D. Oikonomou, K. Simyrdanis, and M. H. Loke. 2021. "Practical Considerations for Shallow Submerged Archaeological Prospection With 3-D Electrical Resistivity Tomography." *Archaeological Prospection* 1: 103–123.

Papadopoulos, N. G., G. N. Tsokas, M. Dabas, M. Yi, J. Kim, and P. Tsourlos. 2009. "Three-Dimensional Inversion of Automatic Resistivity Profiling Data." *Archaeological Prospection* 16: 267–278. https://doi.org/10.1002/arp.361.

Papadopoulos, N. G., P. Tsourlos, C. Papazachos, G. N. Tsokas, A. Sarris, and J.-H. Kim. 2011. "An Algorithm for the Fast 3-D Resistivity Inversion of Surface Electrical Resistivity Data: Application on Imaging Buried Antiquities." *Geophysical Prospection* 59: 557–575.

Papadopoulos, N. G., P. Tsourlos, G. N. Tsokas, and A. Sarris. 2006. "2D and 3D Resistivity Imaging in Archaeological Site Investigation." *Archaeological Prospection* 13: 163–181.

Papadopoulos, N. G., P. Tsourlos, G. N. Tsokas, and A. Sarris. 2007. "Efficient ERT Measuring and Inversion Strategies for 3D Imaging of Buried Antiquities." *Near Surface Geophysics* 5: 349–362.

Papadopoulos, N. G., M.-J. Yi, J.-H. Kim, P. Tsourlos, and G. N. Tsokas. 2010. "Geophysical Investigation of Tumuli by Means of Surface 3D Electrical Resistivity Tomography." *Journal of Applied Geophysics* 70, no. 3: 192–205.

Preacco, M. C. 2014. *Augusta Bagiennorum: Storia e Archeologia di Una Città Augustea*. Celid.

Qiang, S., X. Shi, X. Kang, and A. Revil. 2022. "Optimized Arrays for Electrical Resistivity Tomography Survey Using Bayesian Experimental Design." *Geophysics* 87: E189–E203. https://doi.org/10.1190/geo2021-0408.1.

Sambuelli, L., and C. Comina. 2010. "Fast ERT to Estimate Pollutants and Solid Transport Variation in Water Flow: A Laboratory Experiment." *Bollettino di Geofisica Teorica ed Applicata* 51, no. 1: 1–22.

Sandmeier, K. J. 2021. "Reflexw Version 9.5 Windows XP/7/8/10-Program for the Processing of Seismic, Acoustic or Electromagnetic Reflection, Refraction and Transmission Data." Sandmeier Geophysical Research.

Simyrdanis, K., N. Papadopoulos, and D. Oikonomou. 2021. "Computation of Optimized Electrode Arrays for 3-D Electrical Resistivity Tomography Surveys." *Applied Sciences* 11: 6394.

Slob, E. 2004. "Optimal Acquisition and Synthetic Electrode Arrays." *SEG Technical Program Expanded Abstracts* 23, no. 1: 1389–1392. https://doi.org/10.1190/1.1851115.

Stummer, P., H. Maurer, and A. G. Green. 2004. "Experimental Design: Electrical Resistivity Data Sets That Provide Optimum Subsurface Information." *Geophysics* 69: 120–139. https://doi.org/10.1190/1.1649381.

Torrese, P., F. Zucca, S. Martini, et al. 2022. "Ground Truth Validated 3D Electrical Resistivity Imaging of the Archaeological Deposits at Arma Veirana Cave (Northern Italy)." *Journal of Quaternary Science* 37: 1112–1132. https://doi.org/10.1002/jqs.3406.

Trinks, I., A. Hinterleitner, W. Neubauer, et al. 2018. "Large-Area High-Resolution Ground-Penetrating Radar Measurements for Archaeological Prospection." *Archaeological Prospection* 25: 171–195. https://doi.org/10.1002/arp.1599.

Tsourlos, P., N. Papadopoulos, M.-J. Yi, J.-H. Kim, and G. Tsokas. 2014. "Comparison of Measuring Strategies for the 3-D Electrical Resistivity Imaging of Tumuli." *Journal of Applied Geophysics* 101: 77–85.

Uhlemann, S., P. B. Wilkinson, H. Maurer, F. M. Wagner, T. C. Johnson, and J. E. Chambers. 2018. "Optimised Survey Design for Electrical Resistivity Tomography: Combined Optimisation of Measurement Configuration and Electrode Placement." *Geophysical Journal International* 214: 108–121. https://doi.org/10.1093/gji/ggy128.

Vásconez-Maza, M. D., P. Martínez-Pagán, H. Aktarakçi, M. C. García-Nieto, and M. A. Martínez-Segura. 2020. "Enhancing Electrical Contact with a Commercial Polymer for Electrical Resistivity Tomography on Archaeological Sites: A Case Study." *Materials* 13: 5012. https://doi.org/10.3390/ma13215012.

Vergnano, A., P. De Vingo, G. Rosso, S. Uggè, and C. Comina. 2025. "Integration of Satellite and Aerial Images With Multichannel GPR Surveys in the Archaeological Area of Augusta Bagiennorum for an Improved Description of the Urban Setting." *Journal of Applied Geophysics* 232: 105579. https://doi.org/10.1016/j.jappgeo.2024.105579.

Wilkinson, A. J., E. W. Randall, T. M. Long, and A. Collins. 2006. "The Design of an ERT System for 3D Data Acquisition and a Quantitative Evaluation of Its Performance." *Measurement Science and Technology* 17: 2088–2096. https://doi.org/10.1088/0957-0233/17/8/006.

Wilkinson, P. B., M. H. Loke, P. I. Meldrum, et al. 2012. "Practical Aspects of Applied Optimised Survey Design for Electrical Resistivity Tomography: Applied Optimised ERT Survey Design." *Geophysical Journal International* 189: 428–440. https://doi.org/10.1111/j.1365-246X.2012.05372.x.

Wilkinson, P. B., S. Uhlemann, P. I. Meldrum, et al. 2015. "Adaptive Time-Lapse Optimized Survey Design for Electrical Resistivity Tomography Monitoring." *Geophysical Journal International* 203: 755–766. https://doi.org/10.1093/gji/ggv329.

Witten, A. J. 2017. *Handbook of Geophysics and Archaeology*. 1st ed. Routledge. https://doi.org/10.4324/9781315093260.

Wunderlich, T., and W. Rabbel. 2013. "Absorption and Frequency Shift of GPR Signals in Sandy and Silty Soils: Empirical Relations Between Quality Factor Q, Complex Permittivity and Clay and Water Contents." *Near Surface Geophysics* 11, no. 2: 117–128. https://doi.org/10.3997/1873-0604.2012025.

Supporting Information

Additional supporting information can be found online in the Supporting Information section. **Data S1:** Supporting information. **Data S2:** Supporting information. **Data S3:** Supporting information. **Data S4:** Supporting information. **Data S5:** Supporting information. **Data S6:** Supporting information.

10990763, 0, Downloaded from https://onlinelibrary.wiley.com/doi/10.1002/arp.70013 by Politecnico Di Torino Sist. Bibl Del Polit Di Torino, Wiley Online Library on [09/10/2025]. See the Terms and Conditions (https://onlinelibrary.wiley.com/terms-and-conditions) on Wiley Online Library for rules of use; OA articles are governed by the applicable Creative Commons License

Appendix A

Forward Simulations and Sensitivity Analysis

Forward Simulations

Before the acquisition in the test site, forward simulations were performed to understand if the planned acquisition setup was able to detect resistive anomalies with shapes and dimensions similar to those of the expected buried walls, at the expected depths. We adopted the same ResIPy and GMSH software used for the experimental data. A forward mesh was built, including two isolated anomalies, two cuboids with a hole inside, with dimensions similar to the ones expected for buried walls (side length: 5 m; thickness: 0.5 m). They were placed at 0.5 m depth, with their bottoms at 1 m depth. The two anomalies are identical, but one is rotated 45° to later investigate eventual directional biases among the different simulated survey setups and evaluate also the results of a quasi-3D survey over them. For the forward simulations, the anomalies representing the walls had an electrical resistivity of 2000 Ωm, and the background resistivity representing the soil was set to 40 Ωm.

Three survey setups were simulated:

a. a full-3D single acquisition with an 18 × 8 electrode grid (electrode spacing = 2 m in Figure A1a), with the same quadrupole sequence used for the field test, as described in Section 2;

b. a full-3D survey with two acquisitions, the second one with the grid moved in a similar way to what was performed during the later field testing (Figure A1b);

c. a quasi-3D survey, with 16 lines with 18 electrodes each. The quadrupole sequence used was generated by Electre Pro, the proprietary

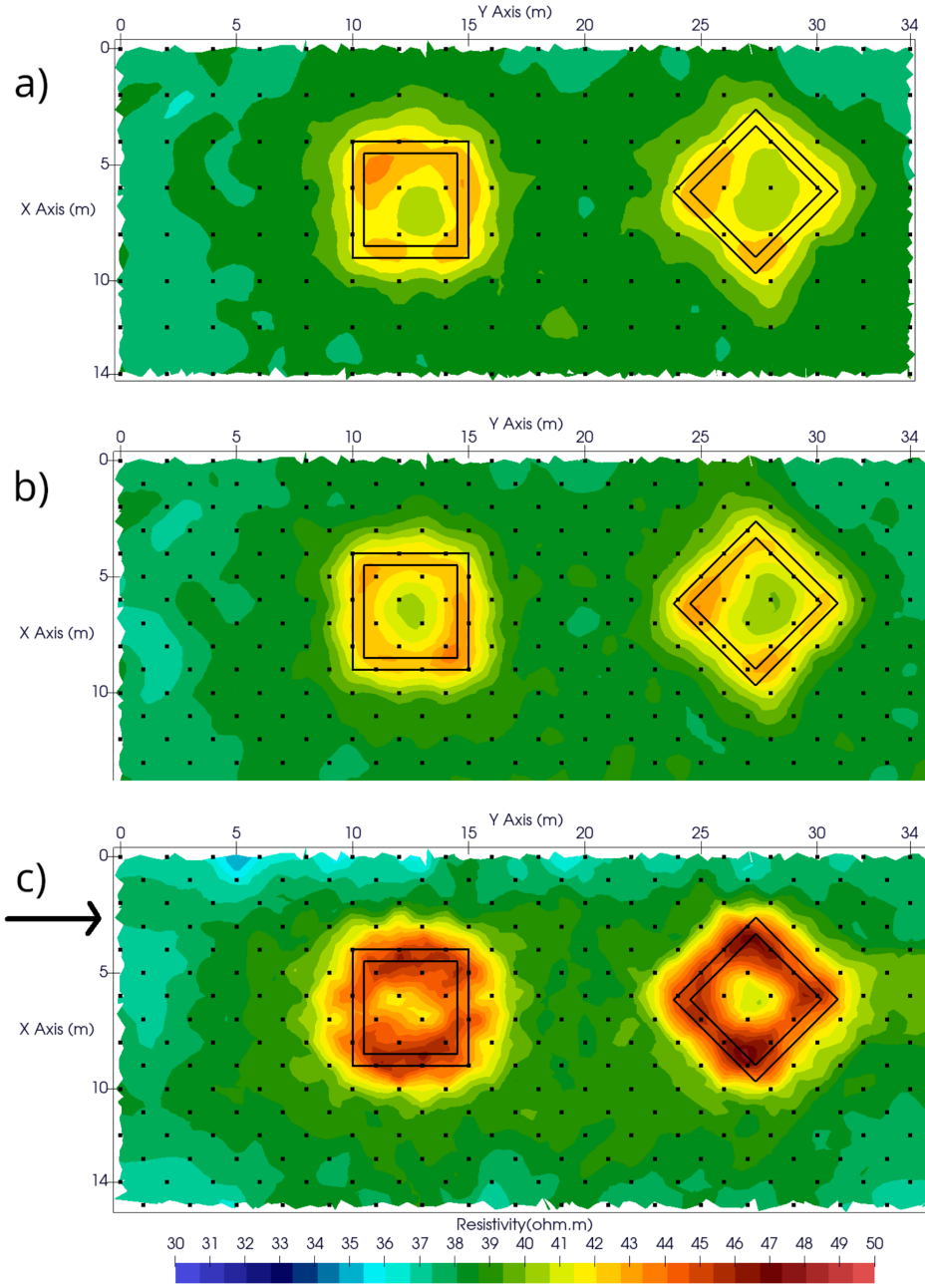


FIGURE A1 | Inversion results of the ERT forward simulations. The simulated resistive anomalies are contoured in black. The black dots represent the positions of the electrodes. Top panel (a): full-3D survey with a single acquisition. Central panel (b): full-3D survey with two acquisitions after a shifting of the acquisition grid similarly to what performed in field surveys. Bottom panel (c): quasi-3D survey with 16 lines of 18 electrodes each (black arrow).

10990763, 0, Downloaded from https://onlinelibrary.wiley.com/doi/10.1002/arp.70013 by Politecnico Di Torino Sist. Bibl Del Polit Di Torino, Wiley Online Library on [09/10/2025]. See the Terms and Conditions (https://onlinelibrary.wiley.com/terms-and-conditions) on Wiley Online Library for rules of use; OA articles are governed by the applicable Creative Commons License

software of the same company of the instrument (IRIS instruments), with default values ($a = 1, 2, 3, 4, 5, 6$; $n = 1, 2, 3$, for a total of 116 measurements per line), as shown in Figure A1c.

The comparison of the obtained results, illustrated in Figure A1, showed that performing the second acquisition could be beneficial in better delineating resistive anomalies of similar dimensions and shapes. Indeed, the shape and dimensions of the anomalies appear more coherent to the simulated anomalies in Figure A1b than in Figure A1a, although in this simulation the improvement is minor. Given the possible advantages, and being logistically simple to manage, we implemented this survey strategy in the field acquisition.

The quasi-3D approach simulated in Figure A1c well resolved the 45°-rotated anomaly, even if it underestimated the anomaly dimensions in the right portion. However, the quasi-3D approach struggled to define the non-rotated anomaly. This is probably due to a directional bias of the setup, which does not include any cross-line measurement; therefore, an anomaly aligned with the survey setup can be smeared in the acquisition direction. This issue is not present in the full-3D approach, which takes advantage of multiple acquisition directions. We also observed that in the quasi-3D survey, an increased contrast in resistivity is obtained between anomalies and background compared with the full-3D one.

However, in all cases, the resistivity values of anomalies are quite far from their real value (2000 Ωm). We observed, during the forward simulations, that changing the resistive anomaly from 2000 to, e.g., 200 000 Ωm, barely modified the pseudosection values. This issue was already noticed and investigated by Berge and Drahor 2011a and is related to the fact that in the presence of resistive anomalies most current lines are concentrated in the less resistive background and are not influenced much by the resistivity values of the resistive anomalies. This is not necessarily a problem for the identification of buried walls; indeed, their shape remains well resolved, but it means that we cannot trust the absolute value of resistivity resulting from the inversion process of field data.

Sensitivity Analysis

The posterior analysis of the resistivity models retrieved after 3D ERT inversion usually involves discussing the sensitivity of the results. This kind of discussion is required because of the inherent non-uniqueness of the inverse solution and allows clarifying how much the resulting model reflects the data (Loke, Chambers, et al. 2013).

A sensitivity section shows the sensitivity of the measured apparent resistivity to the subsurface resistivity model. The higher the sensitivity, the more reliable the resistivity value is. Generally, the sensitivity is high close to the electrodes and near the surface, decreasing with depth and distance from the array. In ResIPy, the sensitivity map is calculated according to Binley and Kemna (2005). It is computed at the end of the inversion if the inversion setting called 'resolution matrix = 1' is selected

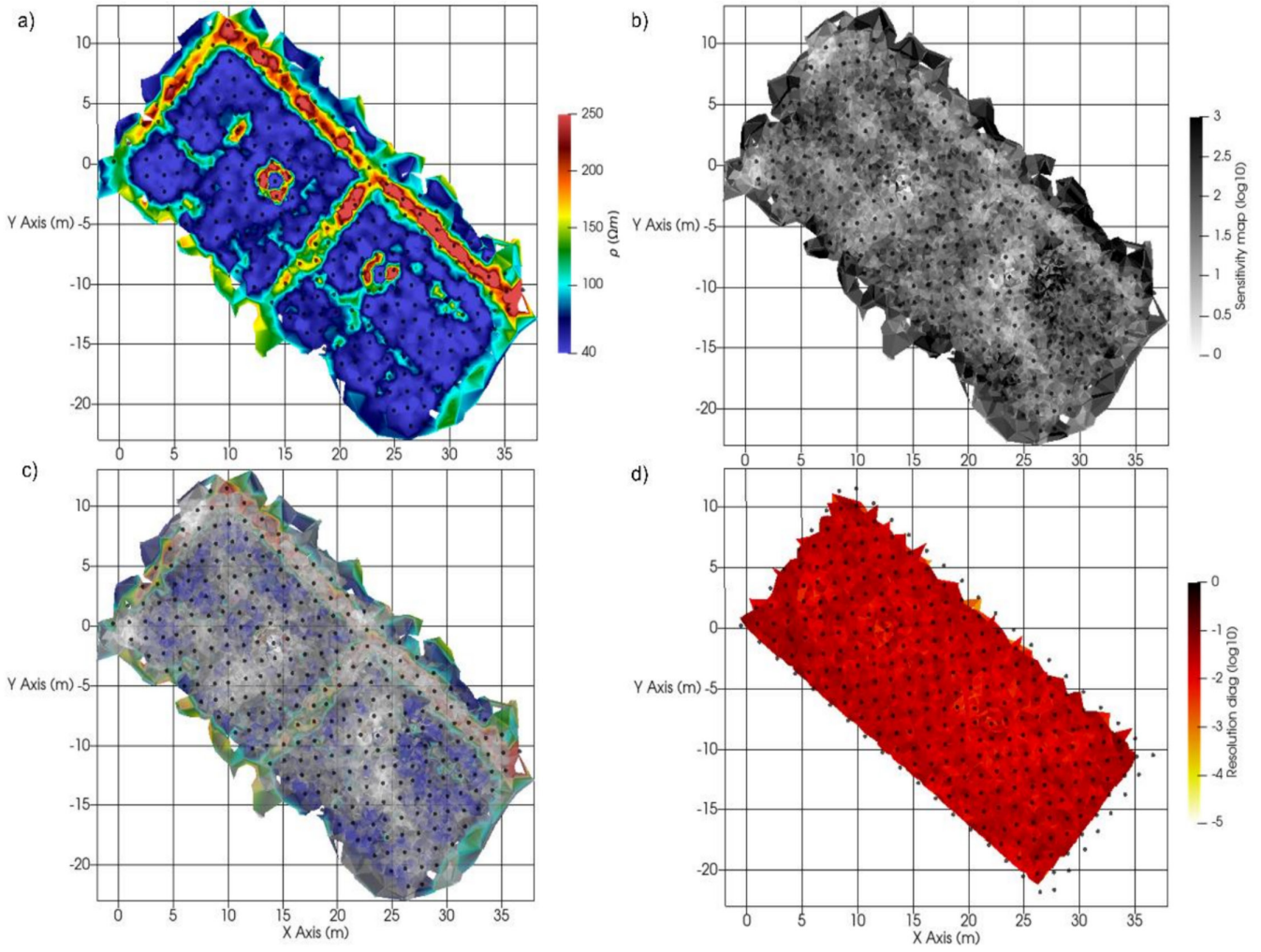


FIGURE A2 | Horizontal slices from the 3D model at a depth of 1 m b.g.l. for: (a) resistivity, (b) sensitivity, (c) overlap of resistivity and sensitivity, (d) diagonal of the resolution matrix.

10990763, 0, Downloaded from https://onlinelibrary.wiley.com/doi/10.1002/arp.70013 by Politecnico Di Torino Sist. Bibl Del Polit Di Torino, Wiley Online Library on [09/10/2025]. See the Terms and Conditions (https://onlinelibrary.wiley.com/terms-and-conditions) on Wiley Online Library for rules of use; OA articles are governed by the applicable Creative Commons License

(Binley 2024). The sensitivity map is stored in the output file 'f001_sen.dat' of ResIPy, available in the Supporting Information ('inversions' folder).

An alternative way for sensitivity evaluation is the model resolution method, which is computationally demanding in 3D but more robust and less affected by the inversion settings used. This method is based on calculating the resolution matrix, whose diagonal elements give the resolution of the model cells (Binley and Kemna 2005). In an ideal case of perfect resolution, the diagonal values should be equal to 1 (logarithm equal to 0), while negative values indicate the effect of adjacent parameters (Loke 2004). In ResIPy, the resolution matrix is calculated if the inversion setting called 'resolution matrix = 2' is selected (Binley 2024), and its diagonal is stored in the output file 'f001_rad.dat', also available in the Supporting Information ('inversions' folder). Both cited methods were adopted for an evaluation of the reliability of the experimental

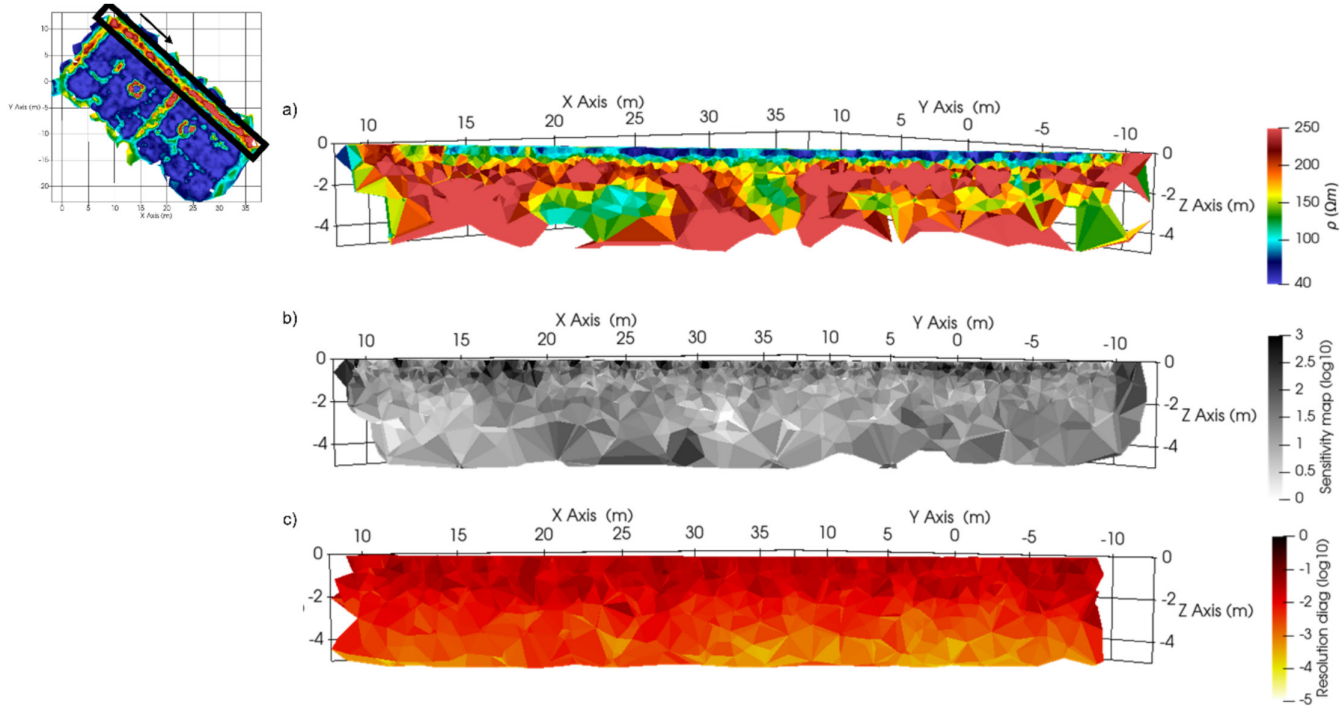


FIGURE A3 | Vertical slices from the 3D model below the outer wall for: (a) resistivity, (b) sensitivity, (c) diagonal of the resolution matrix.

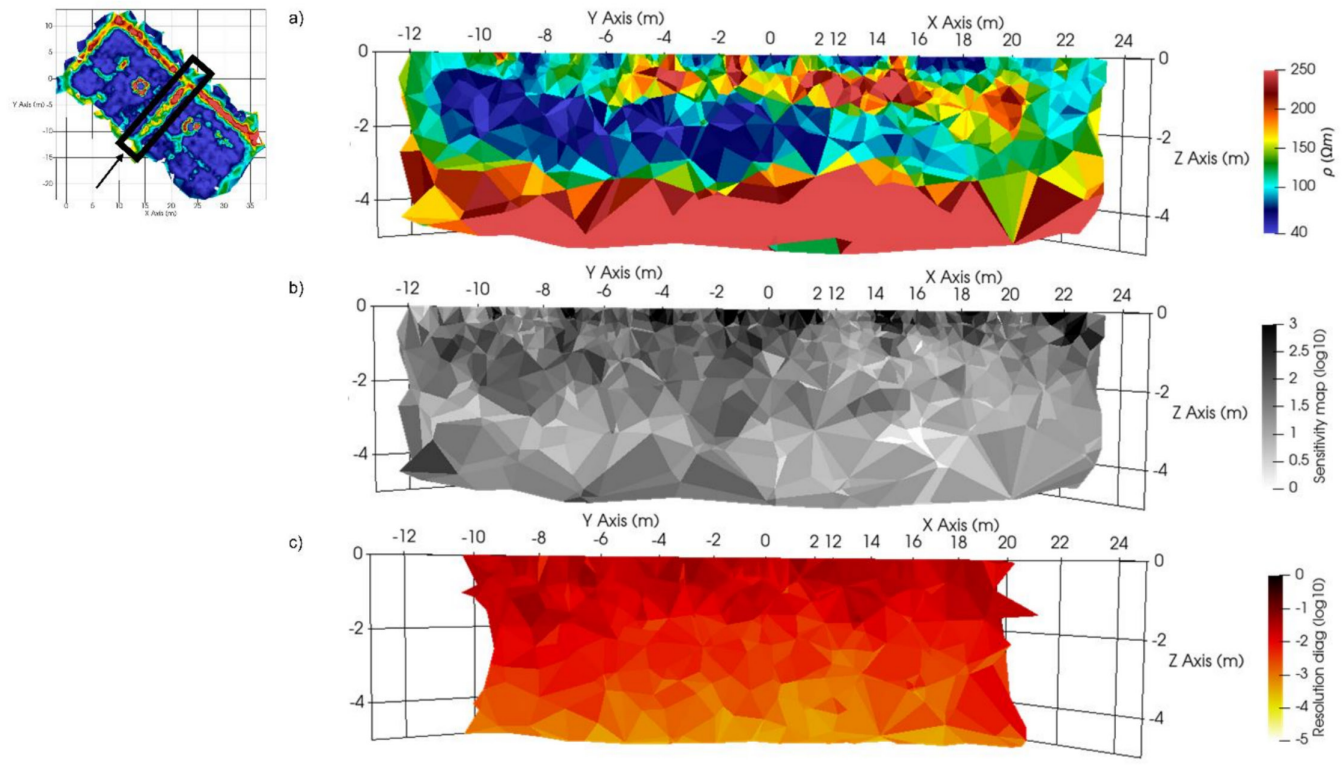


FIGURE A4 | Vertical slices from the 3D model below the inner wall for: (a) resistivity, (b) sensitivity, (c) diagonal of the resolution matrix.

10990763, 0, Downloaded from https://onlinelibrary.wiley.com/doi/10.1002/arp.70013 by Politecnico Di Torino Sist. Bibl Del Polit Di Torino, Wiley Online Library on [09/10/2025]. See the Terms and Conditions (https://onlinelibrary.wiley.com/terms-and-conditions) on Wiley Online Library for rules of use; OA articles are governed by the applicable Creative Commons License

results. Figure A2 plots, at a depth of 1 m b.g.l., the horizontal slices of: resistivity (Figure A2a), sensitivity (Figure A2b), an overlap of them (Figure A2c) and the diagonal of the resolution matrix (Figure A2d). It can be observed that the sensitivity is generally satisfactory. Reduced values are observed in correspondence with the resistive anomalies of the outer and inner walls. Regions with high resistivity have low sensitivity because of less current penetration. Therefore, it can be concluded that the shape of these anomalies can be considered reliable, but their absolute resistivity values could be uncertain.

To better evaluate the variation of sensitivity and reliability with depth of the inverted model, vertical sections of the model below the outer wall (Figure A3) and the inner wall (Figure A4) are reported for resistivity (panels a), sensitivity (panels b) and diagonal values of the resolution matrix (panels c). It can be observed that both the sensitivity and the diagonal of the resolution matrix remain at acceptable values till about 3–4 m depth and then strongly reduce. At these deeper depths, the resistivity models (panels a) also show high resistivity artefacts that should not be considered reliable.

The resolution matrix was calculated separately for the first and second ERT acquisitions because the full computation of it appeared to be too computationally demanding. Figure A5 presents the diagonal of the resolution matrix at different depths, from 0 to −10 m b.g.l. (Figure A5a–d, respectively). This resolution matrix is related to the inversion of the data belonging to the first ERT acquisition. The resolution matrix for the second ERT acquisition was computed as well and resulted in a matrix highly similar to that of the first acquisition (not shown here).

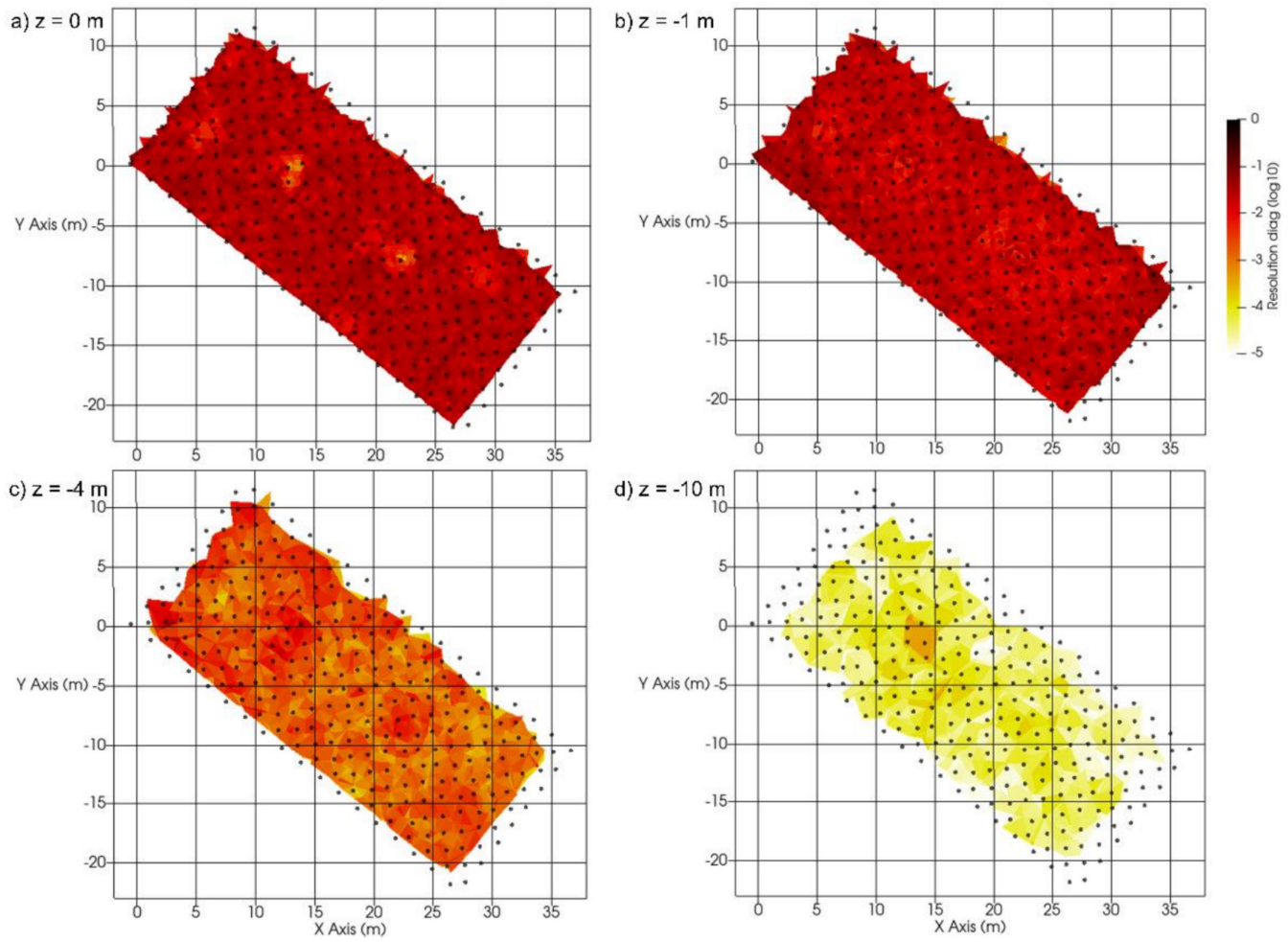


FIGURE A5 | Horizontal slices from the 3D model of the diagonal of the resolution matrix at different depths (b.g.l.): (a) 0 m, (b) −1 m, (c) −4 m, (d) −10 m.

10990763, 0, Downloaded from https://onlinelibrary.wiley.com/doi/10.1002/arp.70013 by Politecnico Di Torino Sist. Bibl Del Polit Di Torino, Wiley Online Library on [09/10/2025]. See the Terms and Conditions (https://onlinelibrary.wiley.com/terms-and-conditions) on Wiley Online Library for rules of use; OA articles are governed by the applicable Creative Commons License